Sum-Frequency Generation at interfaces: a Fresnel story III. Origin of pseudo-resonant processes in centrosymmetric bulks

Bertrand Busson

Sum-Frequency Generation at interfaces: a Fresnel story

III. Origin of pseudo-resonant processes in centrosymmetric bulks

Bertrand Busson

Université Paris-Saclay, CNRS, Institut de Chimie Physique, UMR 8000, 91405 ORSAY, France[a)]

(Dated: 13 June 2023)

The properties of the bulk contribution to Sum-Frequency Generation reflected and transmitted by a finite layer in a multilayer system are described. The leading term is essentially due to the processes emitting in the transmission geometry, in particular for macroscopic layers. For such transmission processes, phase mismatch leads to the production of interference fringes when the layer thickness or a wavelength is tuned, which may be mistaken for resonant processes inside or at the surface of the material. Experimental evidence of such fringes measured from centrosymmetric bulks is provided for a diamond window in the far infrared, and suggested for other materials in previously published data. The existence of a stationary point in the phase mismatch, related to the group velocity mismatch, is shown to be the source of another pseudo-resonant process in centrosymmetric calcium and barium fluorides, for which theoretical predictions reproduce the experimental observations.

[a)]Electronic mail: bertrand.busson@universite-paris-saclay.fr

I. INTRODUCTION

The surface versus bulk duality of the second-order nonlinear processes at interfaces has been elaborated on since the beginning of nonlinear optics.[1–3] For second harmonic generation (SHG), the bulk terms are conveniently mixed with surface ones into a common formalism.[4,5] For Sum-Frequency Generation (SFG), two tracks have been followed to describe the semi-infinite bulk contribution. From the original derivation of Bloembergen and Pershan,[1] a general formulation of SFG emission from a bulk polarization has been developed, separately from the surface response. Details on the source of this polarization have led to models for a free electron gas[6], then generalized to any polarizable material[7] and applied to the difficult case of gold in the visible range.[8,9] On the other hand, equivalence between bulk and surface terms have early been figured out,[10] and widely applied thereafter to simplify the handling of the bulk contribution in the surface spectroscopy frame: in Shen group in the first place,[11–13] then more universally, in particular for the separation between surface and bulk contributions,[14,15] and for the integration into the second order response of the third order bulk contribution driven by a static electric field.[16,17] Both interpretations of the bulk contribution have recently been explicitly reconciled.[18]

In the literature, attention is most of the times paid to SFG bulk contributions when they produce signals of the same order of magnitude as the surface ones, or even higher, and separation between them becomes an issue.[11,18] This is commonly the case for non-centrosymmetric crystals,[12,15] chiral bulks[19,20] and metals.[6,9] Influence of bulk contributions has also been stressed for the liquid water surface: even if they remain rather small,[21] attention has been drawn on their dependence on the interfacial field, which may be modified using electrochemical control or ions.[22] Apart from the obvious particular cases listed above, only few publications have experimentally investigated the bulk response of centrosymmetric materials because most SFG users are interested in the reflection geometry, for which the bulk terms appear much smaller than in transmission.[23] It could be concluded that it is most of the times pointless to focus on the bulk contributions from a transparent centrosymmetric material. However, it must be kept in mind that such materials are precisely what experimenters use for windows and prisms in the SFG set-ups, as well as for substrates, expecting their nonresonant background to remain below the detection threshold. In addition, back reflections may send any bulk SFG produced in a transmission geometry back to the detection

line for reflected SFG. Some unwanted bulk contribution may thus spoil the expected SFG signals from molecular monolayers, even without the experimenter's knowing. Establishing the conditions favourable to these bulk terms (or leading to their extinction) and the rules they follow as a function of adjustable experimental parameters, like film thickness or angles of incidence, helps highlight and control them.

In the two previous papers of this series,[24,25] we have shown that the surface nonlinear response, measured in the far field, of a nonlinear sheet in a stratified N-layer medium was in all cases governed by universal equations (Eq. A1-A5). On the one hand, the nonlinear process itself (driven by the second order susceptibility $\chi^{(2)}$) is independent on the complexity of the interface (number N, thicknesses $d^{[j]}$ and indices of refraction $n^{[j]}$ of the media composing the system) and on the location (i.e. depth inside the system) of the nonlinear sheet. On the other hand, all these constitutive elements and details of the interface are taken into account by the sole Fresnel factors governing the transfer from the far field to the local field. The Fresnel factors thus transform the local hyperpolarizability into an effective one, which acts as an equivalent (and virtual) source of nonlinear polarization emitting SFG radiation just as if the interface was only composed of a freestanding nonlinear sheet surrounded by two semi-infinite media. The case of several interfering nonlinear sheets is easily obtained by summing the individual contributions in amplitude and phase.

In the present article, we address the case where one of the media is nonlinear as a whole, and therefore generates a bulk SFG response. The symmetry properties of this bulk contribution differ from the surface ones. SFG may stem from a dipolar hyperpolarizability, allowed by the bulk symmetries (e.g. non-censtrosymmetric crystals,[15] chiral liquids[26]). But the dipolar components vanish for isotropic or even cubic materials.[3] In these situations, the bulk SFG signals arise from higher order contributions like magnetic and quadrupolar terms.[13] It has long been known that these higher order terms involving magnetic polarizations and quadrupole moments may be recast into a dipolar polarization.[27] The bulk SFG response is thus the output of a nonlinear polarization wave travelling into the medium. In addition, under the hypothesis that the electromagnetic fields are plane waves, all fields in the bulk and their gradients are proportional to the electric field amplitudes.[7] It is therefore possible, in a very general way, to define a dipolar nonlinear susceptibility tensor $\boldsymbol{\chi}_B$ for the bulk which groups together all the contributions.

We first extend the well-known equivalence between bulk and surface contributions from

a semi-infinite bulk to the more general situations of the last semi-infinite medium of an N-layer system, and of a generic layer in such a system as soon as its thickness becomes negligible as compared to the wavelengths (or inverse wavevectors) of all light beams. For bulk generation from a finite thick layer [k], we show that there is strictly speaking no equivalence to a surface contribution, except when only the leading term is considered and the others discarded. This approximation is usually very good for transmitted SFG, all the more when the bulk layer is macroscopic. In this latter situation, the SFG generation process in the bulk may be split between the two subsystems sandwiching layer [k] and the equivalent surface susceptibility mimicking the bulk process depends on the layer thickness and wavevector phase mismatch. Alternatively, the SFG process in transmission from a macroscopic bulk layer becomes equivalent to two out-of-phase surface terms located at each boundary of the layer. This creates interference effects in the bulk contributions, which are experimentally shown to follow the theoretical predictions in a transparent diamond window. We also reconsider previously published SFG spectra measured through a calcium fluoride window or at the surface of silica wafers, for which we propose an alternate explanation in terms of oscillations of the bulk response. Finally, further development of this description provides an explanation to the experimental signals, looking like resonances but of unknown nature so far, observed recently through calcium fluoride crystals, as a consequence of frequency dispersion in the short laser pulses involved in the SFG process.

II. SEMI-INFINITE BULK CONTRIBUTION

In this Part, we examine SFG emitted in reflection by a semi-infinite bulk defined as the last medium of an N-layer system (as sketched in Fig. 1). As the simplest case, we first consider the 2-layer system, i.e. a simple interface between two semi-infinite media [1] and [2], and start by evaluating the SFG field produced by a single sheet located in medium [2] at depth $z = -z_0$. We use Eq. (A1)-(A3) and plug in Eq. (A6)-(A8) where layer [3] is removed by setting $r_{s/p}^{23} = 0$. We recover the Fresnel factors in the two-layer system with fields evaluated inside layer [2], i.e. superscripts $(2L-)$, and write

$$\begin{aligned}\chi_{eff}^{(2)} &= \sum_{\alpha\beta\gamma} F_\alpha^{2L-}(\omega_3) e_\alpha^{[1]}(\omega_3)\, F_\beta^{2L-}(\omega_1) e_\beta^{[1]}(\omega_1)\, F_\gamma^{2L-}(\omega_2) e_\gamma^{[1]}(\omega_2)\, \chi_{\alpha\beta\gamma}^{(2)} e^{i(\Delta k_{z,R}^{[2]})z_0} \\ &= \chi_{eff}^{(2)}(z_0 = 0^-) e^{i(\Delta k_{z,R}^{[2]})z_0} \end{aligned} \quad (1)$$

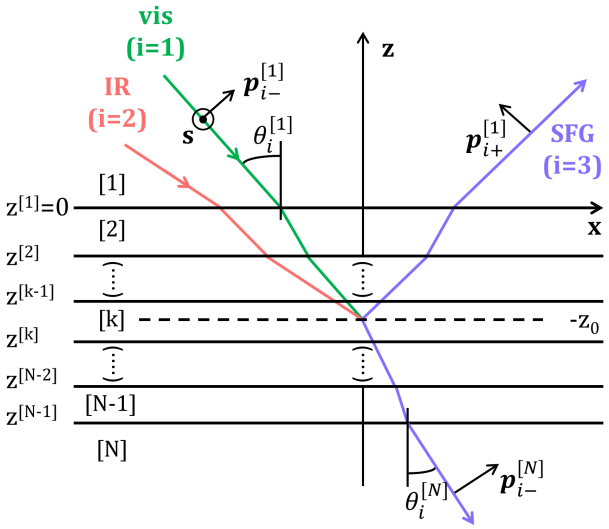

FIG. 1. Sketch of the bulk SFG process in layer [k] of the N-layer system. Multiple reflected, refracted and transmitted rays are not shown for clarity. Thickness $d^{[k]}$ of each layer is equal to $z^{[k-1]} - z^{[k]}$, where $z^{[j]} < 0$ is the depth of interface {j} between media [j] and [j+1].

where $\Delta k_{z,R}^{[2]}$ is the phase mismatch of the SFG process in medium [2] in the reflection geometry, defined as $\Delta k_{z,R}^{[2]} = k_{1,z}^{[2]} + k_{2,z}^{[2]} + k_{3,z}^{[2]}$ where $k_{i,z}^{[2]} = \frac{\omega_i}{c} n_i^{[2]} \cos\theta_i^{[2]}$. This result means that, when medium [2] becomes semi-infinite, the emission at depth $z = -z_0$ is identical to the emission at depth $z = 0^-$ modulated by a phase matching term evaluated at depth $z = -z_0$. We may rewrite this into[28]

$$\chi_{eff}^{(2)} = \int_{-\infty}^{0} \chi_{eff}^{(2)}(z_0 = 0^-) e^{-i(\Delta k_{z,R}^{[2]})z} \delta(z + z_0) dz = \int_{-\infty}^{0} \chi_{eff,B}^{(2)}(z) e^{-i(\Delta k_{z,R}^{[2]})z} dz \qquad (2)$$

where we define as usual[10,24] the effective bulk susceptibility $\chi_{eff,B}^{(2)}(z) = \chi_{eff}^{(2)}(z_0 = 0^-)\delta(z + z_0)$ or, equivalently, $\boldsymbol{\chi}_B^{(2)}(z) = \boldsymbol{\chi}^{(2)}(z_0 = 0^-)\delta(z + z_0)$. In Ref. 29, a discrete (instead of continuous) distribution of thin layers was used for the integration.

If we now consider that the whole medium [2] acts as a nonlinear source, we replace the δ-distribution at $z = -z_0$ by a uniform distribution $\boldsymbol{\chi}_B^{(2)}(z) = \boldsymbol{\chi}_B^{(2)}$ constant over medium [2]. Equation 2 shows that we may define an equivalent surface second-order susceptibility, located at $z = 0^-$, by

$$\chi_{eff}^{(2)} = \int_{-\infty}^{0} \chi_{eff,B}^{(2)} e^{-i(\Delta k_{z,R}^{[2]})z} dz = \chi_{eff,B}^{(2)} \frac{i}{\Delta k_{z,R}^{[2]}} \qquad (3)$$

In other words, the SFG emitted by the semi-infinite bulk with bulk susceptibility $\boldsymbol{\chi}_B^{(2)}$ is equal to that emitted by a surface polarization given by $i\boldsymbol{\chi}_B^{(2)}/\Delta k_{z,R}^{[2]}$, located at the

interface inside medium [2].[18] We recover the original conclusions of Ref. 10 under the same hypotheses: a dipolar source for the bulk contribution excited by light modelled by plane waves. This equivalence has proved very useful for the analysis of the bulk contribution of water at a free or charged interface.[16,17,30]

When the semi-infinite bulk is defined as layer [3] in a three-layer system, we have for each Fresnel factor at depth $z = -z_0$ inside medium [3] (with $z_0 \geqslant D$, where D is the usual notation for thickness $d^{[2]}$), noting α_i = x, y or z:

$$F_{\alpha_i}(\omega_i, z_0) = F_{\alpha_i}^{3L-}(\omega_i, z = -D) e^{ik_{i,z}^{[3]}(z_0 - D)}. \tag{4}$$

Following the same procedure as in the 2-layer system, we set

$$\chi_{eff}^{(2)} = \int_{-\infty}^{-D} \chi_{eff}^{(2)}(z = -D) e^{-i\Delta k_{z,R}^{[3]}(z+D)} \delta(z + z_0) dz = \int_{-\infty}^{0} \chi_{eff,B}^{(2)}(z') e^{-i(\Delta k_{z,R}^{[3]})z'} dz' \tag{5}$$

with $\chi_{eff,B}^{(2)}(z') = \chi_{eff}^{(2)}(z = -D)\delta(z' + z_0 - D)$. To reconstruct the bulk, we set $\boldsymbol{\chi}_B^{(2)}(z')$ constant over $z' \leqslant 0$. As above, SFG emission by the semi-infinite bulk becomes equivalent to that produced by a surface susceptibility $i\boldsymbol{\chi}_B^{(2)}/\Delta k_{z,R}^{[3]}$ located at $z = -D$ in medium [3]. Here, only the phase mismatch generated by beam propagation in medium [3] appears in the definition of the equivalent surface susceptibility. Phase mismatch and Fabry-Pérot interference in medium [2] come separately out when $F_{\alpha_i}^{3L-}(\omega_i, z = -D)$ is evaluated using Eq. A6-A8, to calculate the far field emitted towards medium [1] from Eq. A1.

This result generalizes to the SFG emission by a semi-infinite bulk defined as layer [N] in an N-layer system. From Ref. 25, Eq. 4 holds when the various terms at interface {2} and medium [3] are replaced by their counterparts at interface {N-1} and in medium [N], respectively. The phase factor becomes $k_{i,z}^{[N]}(z_0 + z^{[N-1]})$, where $z^{[N-1]} < 0$ defines the last interface of the system. After integration, SFG emitted by this semi-infinite bulk with uniform $\boldsymbol{\chi}_B^{(2)}$ is identically modelled by an equivalent surface susceptibility $i\boldsymbol{\chi}_B^{(2)}/\Delta k_{z,R}^{[N]}$ located inside medium [N] at $z = z^{[N-1]}$.

III. BULK CONTRIBUTION FROM A FILM OF FINITE EXTENT

A. General results

We note that the results of the previous Part are not relevant when the bulk nonlinear medium is not the last one in the N-layer system, as a consequence of the Fabry-Pérot effects

generated by the reflections at its boundaries. Comparing Eq. A6-A17 and A18-A29, we see that the z_0-dependences of the Fresnel factors in a generic layer [k] inside the N-layer system and in layer [2] inside the three-layer system are analogous. We therefore focus on the archetype bulk layer [2] (located between $z = 0$ and $z = -D$) in the three-layer case as a representative of the general N-layer system, to which the results established in this Part identically apply. Whatever the polarization, the expressions of the fields at arbitrary depth $z = -z_0$ in Eq. A6-A8 involve the sum of a downgoing and an upgoing wave,[29] as evidenced by their phases evolving as $e^{ik_{i,z}^{[2]}z_0}$ and $e^{-ik_{i,z}^{[2]}z_0}$, respectively. We rewrite these local Fresnel factors for $\alpha_i = x, y, z$ as:

$$F_{\alpha_i}^{film}(\omega_i) = A_{\alpha_i}(\omega_i, D)\left[e^{ik_{i,z}^{[2]}z_0} + B_{\alpha_i}(\omega_i)e^{2i\beta_i}e^{-ik_{i,z}^{[2]}z_0}\right] \tag{6}$$

where $B_{\alpha_i}(\omega_i)$ terms are essentially reflection coefficients $r_{s/p}^{23}(\omega_i)$ and bear the $-ik_{i,z}^{[2]}z_0$ phase factors of the upgoing wave. For SFG measured in transmission, the Fresnel factors for the SFG beam become (Eq. A12-A14):

$$F_{\alpha_3}^{film,T}(\omega_3) = A_{\alpha_3}^{T}(\omega_3, D)\left[e^{-ik_{3,z}^{[2]}z_0} + B_{\alpha_3}^{T}(\omega_3)e^{ik_{3,z}^{[2]}z_0}\right] \tag{7}$$

As detailed in the Appendix, for layer [k] inside the N-layer system, Eq. 6 and 7 still apply with factors $A_{\alpha_i}(\omega_i)$ and $B_{\alpha_i}(\omega_i)$ now depending on all thicknesses $d^{[j]}$. We write them for short $A_{\alpha_i}(\omega_i, d^{[k]})$ and $B_{\alpha_i}(\omega_i, d^{[k]})$. Expressions for $A_{\alpha_i}(\omega_i, d^{[k]})$ are shown in the Appendix, whereas expressions for $B_{\alpha_i}(\omega_i, d^{[k]})$ are complicated by the ruled product.

When the three beams are taken into account, the product of the Fresnel factors appearing in Eq. A3 generates eight terms[20] with different phase mismatches $(\pm k_{3,z}^{[2]} \pm k_{1,z}^{[2]} \pm k_{2,z}^{[2]})z_0$, labelled $\Delta k_{z,\{\pm\pm\pm\}}^{[2]}z_0$,[31] for example $\Delta k_{z,\{-+-\}}^{[2]}$ for the $(-k_{3,z}^{[2]} + k_{1,z}^{[2]} - k_{2,z}^{[2]})z_0$ term weighted by $B_{\alpha_3}(\omega_3)B_{\alpha_2}(\omega_2)e^{2i(\beta_3+\beta_2)}\prod_{i=1}^{3}A_{\alpha_i}(\omega_i)$. When layer [2] becomes the source of bulk SFG between $z = -D$ and $z = 0$, the result of the previous Part is generalized by factoring the terms depending on z_0 and using identities like

$$e^{i(\Delta k_{z,\{\pm\pm\pm\}}^{[2]})z_0} = \int_{-D}^{0} e^{-i(\Delta k_{z,\{\pm\pm\pm\}}^{[2]})z}\delta(z + z_0)dz, \tag{8}$$

then replacing the Dirac distribution at $-z_0$ by a constant bulk susceptibility. After integration between $-D$ and 0 as in Eq. 3, each term has a different behaviour as for the relationship between bulk susceptibility and its equivalent surface susceptibility, appearing

as a factor

$$\frac{i\left(1-e^{i\Delta k^{[2]}_{z,\{\pm\pm\pm\}}D}\right)}{\Delta k^{[2]}_{z,\{\pm\pm\pm\}}} = D\, e^{i\Delta k^{[2]}_{z,\{\pm\pm\pm\}}D/2}\,\mathrm{sinc}\left(\Delta k^{[2]}_{z,\{\pm\pm\pm\}}D/2\right) \tag{9}$$

where we introduce function $\mathrm{sinc}(x) = \sin(x)/x$, commonly encountered in phase matching analysis.[32–35] These formulas generalize to the N-layer system by introducing $\Delta k^{[k]}_{z,\{\pm\pm\pm\}}(z_0 + z^{[k-1]})$ instead of $\Delta k^{[2]}_{z,\{\pm\pm\pm\}}z_0$, and integrating between $z^{[k-1]}$ and $z^{[k]}$ to recover $d^{[k]}$. In Eq. 9, there appears to be no simple relationship common to all eight terms, and no general behavior can be established for their sum. In particular, the presence of the denominators prevents from retrieving products of complete Fresnel factors (Eq. 6 and 7) when summing them up, and the total effective polarization emitting bulk SFG is here not equivalent to a surface nonlinear polarization. Recovering the formal expression of the complete Fresnel factors serves indeed as a criterion for the transformation of bulk SFG into an equivalent surface SFG, as was for example made explicit in Ref. 18.

B. Extension to Sum-Frequency scattering

Throughout this article series, the interface has been described as a stack of layered media separated by infinite plane and parallel interfaces. In this section we consider how Fresnel factors may influence the Sum-Frequency scattering process.[36]

1. Equivalence between phase-matched and scattered SF emission

Briefly, we consider an individual object of arbitrary shape, with a characteristic size of a few tens of nanometers or more, interacting with the same incoming light beams as in Fig. 1. The essential difference lies in the fact that SFG radiation is now scattered by the object in any direction, defined by a wavevector $\boldsymbol{k}$, because the phase-matching condition [Eq. A2] is specific to the plane multilayer system and does not apply here. The effective susceptibility[37] $\boldsymbol{\Gamma}^{(2)}$ for scattering differs from Eq. A3 (or Eq. A5) for several reasons. In Eq. A3, the effective susceptibility sums up into a scalar quantity the projections of the local susceptibility $\boldsymbol{\chi}^{(2)}$, linked to the symmetries of the interface, onto the incoming and outgoing (fixed) polarization vectors (hence the decomposition into x, y and z components in Eq. A6-A8). In a scattering experiment, the far field intensity is measured in the direction

of $\boldsymbol{k}$, which is not fixed (hence Eq. A4 is modified). The effective susceptibility has to be re-projected onto the scattering frame (linked to $\boldsymbol{k}$), so $\mathbf{\Gamma}^{(2)}$ is expressed as a tensor quantity. In addition, the local susceptibility and its projections onto polarization vectors $\boldsymbol{e}$ now vary with the point considered on the object, and, for large objects, so do the phases of the three beams. The effective susceptibility tensor $\mathbf{\Gamma}^{[2]}$ thus integrates over the object all these local variations (we neglect nonlocal contributions):

$$\Gamma^{[2]}_{\alpha\beta\gamma}(\boldsymbol{q}) = \int_V \sum_{\mu\nu\xi} [F_\alpha(\omega_3,\boldsymbol{r})\boldsymbol{e}_\alpha]_\mu \, \chi^{(2)}_{\mu\nu\xi}(\boldsymbol{r}) [F_\beta(\omega_1,\boldsymbol{r})\boldsymbol{e}^{[1]}_\beta]_\nu [F_\gamma(\omega_2,\boldsymbol{r})\boldsymbol{e}^{[1]}_\gamma]_\xi \, e^{i\boldsymbol{q}\cdot\boldsymbol{r}} d^3\boldsymbol{r} \tag{10}$$

where $\boldsymbol{q} = \boldsymbol{k} - (\boldsymbol{k}_1 + \boldsymbol{k}_2)$ is the scattering vector, which has a form analogous to $\Delta k^{[2]}_{z,\{+--\}}$. As they transfer the far field to the local field, Fresnel factors account here for the boundary conditions at the surface of the object, the choice for $\boldsymbol{e}_\alpha(\omega_3)$ depending on the medium in which the scattered intensity is measured in the far field. For a spherical object, the components of tensor $\mathbf{\Gamma}^{[2]}$ may be calculated.[38] For dielectric (e.g. liquid) droplets,[36,39] the Rayleigh-Gans-Debye (RGD) approximation is often applied, which states that the light beams are not modified by the presence of the objects. This is equivalent to postulate refractive index matching between the object and its surrounding medium,[40] hence essentially setting Fresnel factor amplitudes to 1. Within this approximation, for isotropic particles, the relationships between $\boldsymbol{\chi}^{(2)}$, $\mathbf{\Gamma}^{(2)}$ and far field intensity becomes simpler.[37,40,41]

As pointed out in the literature,[36] Eq. 10 may also be evaluated when the object is an infinite homogeneous plane layer (between $z = 0$ and $z = -D$ as above) in a multilayer system, to recover the equations specific to the phase-matched situation. In this case, we set $\boldsymbol{\chi}^{(2)}(\boldsymbol{r}) = \Pi(z,-D,0)\,\boldsymbol{\chi}^{(2)}_B$ where $\Pi(z,-D,0)$ is a rectangular function along z, equal to 1 between $-D$ and 0. As boundary conditions evaluated on a plane interface, Fresnel factors become constant, equal to $A_\beta(\omega_1, D)$, $A_\gamma(\omega_2, D)$ and $A^T_\alpha(\omega_3, D)$ for the three beams, respectively. Origin of the phases is taken in medium [1] and factors A_{α_i} include the dephasing up to the scattering layer (Eq. A21-A23), so the origin of the scattering phase $e^{i\boldsymbol{q}\cdot\boldsymbol{r}}$ is at $z = 0$. Eq. 10 becomes

$$\Gamma^{[2]}_{\alpha\beta\gamma}(\boldsymbol{q}) = \sum_{\mu\nu\xi} [A^T_\alpha(\omega_3)\boldsymbol{e}_\alpha]_\mu [\boldsymbol{\chi}^{(2)}_B]_{\mu\nu\xi} [A_\beta(\omega_1)\boldsymbol{e}^{[1]}_\beta]_\nu [A_\gamma(\omega_2)\boldsymbol{e}^{[1]}_\gamma]_\xi \int_V \Pi(z,-D,0)\, e^{i\boldsymbol{q}\cdot\boldsymbol{r}} d^3\boldsymbol{r} \tag{11}$$

Separating the integration between in-plane [$\boldsymbol{r}_\parallel = (x, y)$] and perpendicular (z) components,

the integral becomes

$$\int_V \Pi(z,-D,0)\, e^{i\boldsymbol{q}\cdot\boldsymbol{r}} d^3\boldsymbol{r} = \int_{x,y} e^{i\boldsymbol{q}_\parallel\cdot\boldsymbol{r}_\parallel} d^2\boldsymbol{r}_\parallel \int_z \Pi(z,-D,0) e^{iq_z z} dz \tag{12}$$

The first term is the Fourier transform of a constant function and equals $\delta(\boldsymbol{q}_\parallel)$, which translates into $\boldsymbol{k}_\parallel = (\boldsymbol{k}_1 + \boldsymbol{k}_2)_\parallel = (\boldsymbol{k}_3)_\parallel$ when the total scattered intensity (i.e. integrated over all values of $\boldsymbol{k}$) is calculated. We recognize the phase matching condition, and the SF scattering turns down to the phase-matched process at the planar interface. In addition, using $|\boldsymbol{k}| = |\boldsymbol{k}_3|$, we get $\boldsymbol{k}_z = \pm\boldsymbol{k}_{3,z}$. The two solutions correspond to SFG emitted in transmission (T,+) and reflection (R,-), leading to $iq_z z = -i\Delta k_{z,T}$ and $iq_z z = -i\Delta k_{z,R}$, respectively. Evaluation of the second integral gives the Fourier transform of the rectangular function Π, equal to Eq. 9 evaluated for $\Delta k_{z,T}$ and $\Delta k_{z,R}$, respectively. Finally, we remark that the scattering frame, linked to $\boldsymbol{k}$, becomes equal to the phase-matched frame associated with $\boldsymbol{k}_3$. Projections onto (μ,ν,ξ) identify to projections onto (α,β,γ), so the summation over (μ,ν,ξ) disappears, and we have

$$\Gamma^{[2],R/T}_{\alpha\beta\gamma} = A^{R/T}_\alpha(\omega_3)\boldsymbol{e}^{R/T}_\alpha \boldsymbol{\chi}^{(2)}_{B,\alpha\beta\gamma} A_\beta(\omega_1)\boldsymbol{e}^{[1]}_\beta A_\gamma(\omega_2)\boldsymbol{e}^{[1]}_\gamma D\,\mathrm{sinc}\left(\frac{\Delta k^{[2]}_{z,\{R/T\}} D}{2}\right) e^{i\frac{\beta_1+\beta_2(+/-)\beta_3}{2}} \tag{13}$$

where $(+/-)$ corresponds to R/T, respectively. We recognize the $(\alpha\beta\gamma)$ component of the effective susceptibility (as defined by Eq. A3 and A5), limited to A_{α_i} terms only in Eq. 6 and 7. This, together with the equations governing emission of SFG intensity in the far field as a function of $\Gamma^{[2]}$ in this situation,[37] shows the equivalence of scattering and phase matched description of SFG from a bulk layer in a multilayer system.

2. SF scattering inside an N-layer system

One may wonder why only the A_{α_i} terms are present in Eq. 13, displaying only one of the total eight terms described earlier. This is due to the fact that scattering of the three beams by the object (as a linear optical process) is neglected in the description of SFG nonlinear scattering. When the object is an infinite plane layer, integration of the scattered beams gives birth to the refracted and reflected waves inside and outside the layer. Fresnel factors in Eq. 10 integrate indeed refraction at, and up to, the surface of the object, but cannot take reflection at the exit side of the layer into account as these reflected beams have a different value as for their $k_{i,z}$ components (i.e. different $\boldsymbol{q}$). These reflected beams

correspond to the B_{α_i} terms. This shows that, for a plane layer, it is not possible to neglect this linear scattering effect (the reader may refer to Sections III D and III E, and to Ref. 24-25 describing how B_{α_i} terms may nevertheless be neglected in some cases, for example in macroscopic layers). Conversely, for an arbitrary nanoscale object, it is conceivable to neglect linear scattering in the interpretation of its nonlinear SF scattering. Taking it into account would add other contributions to $\boldsymbol{k}_1$, $\boldsymbol{k}_2$ and $\boldsymbol{k}$, scattered by the object in arbitrary directions in space. This has been addressed in the literature,[38] but for most situations the wavevectors are kept fixed (all the more when the RGD approximation is used).

However, in realistic experimental conditions, such a nanoscale object is embedded in a dispersion medium (matrix, solvent), with finite thickness D, and may be in addition included in a multilayer system. So the complete system in that case is described as a usual N-layer system (so $\boldsymbol{z}$ axis is uniquely defined), where phase-matched SFG may be produced at interfaces or bulks, with one of the layers (the dispersion medium) containing sources of SFG scattering. In that layer, local electric fields also involve beams reflected at its exit boundary $z = -D$, having $-k_{i,z}$ (resp. $-k_z$) components as for their incident (resp. SFG) wavevectors. It is easily checked that accounting for these reflected beams inside Eq. 10, weighted by their amplitudes, turns down to adding seven new terms to Eq. 10, each one carrying its own value for wavevector $\boldsymbol{q} = \boldsymbol{q}_\parallel + q_z\boldsymbol{z}$ inside the object. For each position $\boldsymbol{r}$ at the sample, splitting the phase factor $e^{iq_z z}$ in three terms (corresponding to ω_1, ω_2 and ω_3) allows integrating each of them into the corresponding Fresnel factor. This reconstructs the complete Fresnel factors inside the dispersion medium (Eq. 6 and 7), to the expenses of the uniqueness of scattering vector $\boldsymbol{q}$, whose z-component now may take eight values $q_{\{z,\pm\pm\pm\}}$. Eq. 10 transforms into

$$\Gamma^{[2]}_{\alpha\beta\gamma}(\boldsymbol{q}_\parallel, q_{\{z,\pm\pm\pm\}}) = \int_V \sum_{\mu\nu\xi} \chi^{dressed}_{\mu\nu\xi,\alpha\beta\gamma}(\boldsymbol{r}) e^{i\boldsymbol{q}_\parallel\cdot\boldsymbol{r}_\parallel}\, d^3\boldsymbol{r} \tag{14}$$

where

$$\chi^{dressed}_{\mu\nu\xi,\alpha\beta\gamma}(\boldsymbol{r}) = [F^{film,T}_\alpha(\boldsymbol{r}, -k_z)\boldsymbol{e}_\alpha]_\mu\, \chi^{(2)}_{\mu\nu\xi}(\boldsymbol{r})\, [F^{film}_\beta(\boldsymbol{r}, -k_{1,z})\boldsymbol{e}^{[1]}_\beta]_\nu\, [F^{film}_\gamma(\boldsymbol{r}, -k_{2,z})\boldsymbol{e}^{[1]}_\gamma]_\xi \tag{15}$$

with implicit dependence of the three Fresnel factor on ω_3, ω_1 and ω_2. These equations provide a generalized frame for the analysis of SFG scattering by a nanoscale object dispersed in a finite layer included inside a multilayer system. The total intensity, summing up the contributions of all these individual objects, may involve additional interference effects at

larger scales,[37,42,43] depending on the size, density, separation and relative orientation of the nanoscale objects inside the dispersion medium.

C. Layers with negligible thickness

We go back to the usual phase-matched SFG and consider the results of Part III A in particular cases. When the thickness D of layer [2] is small enough to neglect the Fabry-Pérot and phase matching effects (e.g. $D \ll \lambda_3/2\pi$), it behaves like a zero-thickness layer (i.e. $D \to 0$, $z_0 \to 0$ and $\beta_i \to 1$) and we recover in Eq. 6 and 7 the Fresnel factors of the usual three-layer model.[44] Care must be taken for strongly absorbing materials like metals, for which more stringent conditions on D may apply (e.g. D smaller than the skin depth). Summing up the eight terms, the effective susceptibility of layer [2] becomes

$$\chi^{(2)}_{eff} = D \sum_{\alpha\beta\gamma} e^{[1]}_{\alpha} e^{[1]}_{\beta} e^{[1]}_{\gamma} F^{3L}_{\alpha}(\omega_3) F^{3L}_{\beta}(\omega_1) F^{3L}_{\gamma}(\omega_2) \chi^{(2)}_{B,\,\alpha\beta\gamma} \tag{16}$$

This shows that the bulk SFG emission of such a thin film with bulk susceptibility $\boldsymbol{\chi}^{(2)}_B$ is equal to that generated by an equivalent surface susceptibility $D\,\boldsymbol{\chi}^{(2)}_B$ placed in layer [2]. Using the results of Ref. 25, it is possible to show in the same way that, in an N-layer system, the SFG emitted by the bulk of a thin layer [k], with thickness $d^{[k]} \ll \lambda_3/2\pi$, is equivalently obtained by replacing the bulk susceptibility $\boldsymbol{\chi}_B$ by a surface susceptibility equal to $d^{[k]}\boldsymbol{\chi}^{(2)}_B$ located between layers [k-1] and [k+1]. These conclusions are also valid for SFG emitted in transmission.

There are thus two extreme regimes for which the SFG signal emitted by the bulk of a layer [k] in an N-layer system is equivalent to a single surface SFG signal: for an ultrathin layer [k], with an equivalent surface susceptibility equal to $d^{[k]}\boldsymbol{\chi}^{(2)}_B$, and in reflection from the semi-infinite layer [N], with an equivalent surface susceptibility located at the {N-1,N} interface in medium [N] and equal to $i\boldsymbol{\chi}^{(2)}_B/\Delta k^{[N]}_{z,R}$. We note that, in these two situations, the Fabry-Pérot effects do not apply, giving rise to this equivalence, which is not possible in other cases.

D. Leading contributions

Considering a general layer as in Part III A, the complete bulk SFG response sums up eight terms. Among these, we call "direct process" the term driven by the product $A_{\alpha_3}(\omega_3)A_{\alpha_1}(\omega_1)A_{\alpha_2}(\omega_2)$ (or $A^T_{\alpha_3}(\omega_3)A_{\alpha_1}(\omega_1)A_{\alpha_2}(\omega_2)$ in transmission), involving no internal reflection of one of the beams inside the bulk layer. These eight contributions don't have the same orders of magnitude, as a consequence of their denominators in Eq. 9. The highest one shall naturally be related to the lowest phase mismatch, which is by far $\Delta k^{[2]}_{z,\{-++\}} = k^{[2]}_{1,z} + k^{[2]}_{2,z} - k^{[2]}_{3,z} = \Delta k^{[2]}_{z,T}$ (or equivalently $\Delta k^{[k]}_{z,T}$ in the N-layer system). As a first approximation, this leading term, together with the conjugate $\Delta k^{[2]}_{z,\{+--\}} = -\Delta k^{[2]}_{z,T}$, may become sufficient to describe the bulk response.

1. Transmission geometry

For SFG measured in transmission, selecting the terms driven by $\pm\Delta k^{[2]}_{z,T}$ keeps the direct "downward" contribution, together with the "upward" contribution involving the three reflected beams, and the effective nonlinear susceptibility transforms into

$$\chi^{(2)}_{eff,T} \approx D\,\mathrm{sinc}\left(\frac{\Delta k^{[2]}_{z,T} D}{2}\right) e^{i\frac{\beta_1+\beta_2-\beta_3}{2}} \sum_{\alpha\beta\gamma} \chi^{dressed,T}_{B,\,\alpha\beta\gamma} \tag{17}$$

where

$$\chi^{dressed,T}_{B,\,\alpha\beta\gamma} = e^{[3]}_{\alpha} e^{[1]}_{\beta} e^{[1]}_{\gamma} A^T_{\alpha} A_{\beta} A_{\gamma} \chi^{(2)}_{B,\,\alpha\beta\gamma} \left[1 + B^T_{\alpha} B_{\beta} B_{\gamma} e^{i(\beta_1+\beta_2+\beta_3)}\right] \tag{18}$$

All other terms following from Eq. 9 are minored indeed for two reasons: (i) they scale like their own $1/\Delta k^{[2]}_{z,\{\pm\pm\pm\}}$ where $\Delta k^{[2]}_{z,\{\pm\pm\pm\}} \gg \Delta k^{[2]}_{z,T}$, and (ii) their Fresnel factors involve reflection coefficients B_{α_i}, with magnitudes usually smaller than one. With this second argument, it may also be inferred that the second term in Eq. 18, weighted by a product of three reflection coefficients is, in most situations, much smaller than the direct term. The direct contribution alone is thus a good approximation of bulk SFG emitted in transmission.

2. Reflection geometry

When the reflection geometry is considered, the direct process is discarded because it corresponds to the biggest phase mismatch $\Delta k^{[2]}_{z,R}$ among all $\Delta k^{[2]}_{z,\{\pm\pm\pm\}}$, so its relative weight

[$\sim (1/\Delta k_{z,R}^{[2]})^2$ as for the intensities] is also the smallest. Restricting the sum to the leading $\pm\Delta k_{z,T}^{[2]}$ terms, we get:

$$\chi_{eff}^{(2)} \approx D\,\mathrm{sinc}\left(\frac{\Delta k_{z,T}^{[2]} D}{2}\right) e^{i\frac{\beta_1+\beta_2+\beta_3}{2}} \sum_{\alpha\beta\gamma} \chi_{B,\,\alpha\beta\gamma}^{dressed} \tag{19}$$

with

$$\chi_{B,\,\alpha\beta\gamma}^{dressed} = e_\alpha^{[1]} e_\beta^{[1]} e_\gamma^{[1]} A_\alpha A_\beta A_\gamma \chi_{B,\,\alpha\beta\gamma}^{(2)} \left[B_\alpha e^{i\beta_3} + B_\beta B_\gamma e^{i(\beta_1+\beta_2)}\right] \tag{20}$$

As they are driven by the transmission phase mismatch, these two dominant processes involve SFG measured in reflection but locally produced by interaction of three beams in the transmission geometry, either after reflection of the "downward" SFG beam at the {23} interface (first term in the sum in Eq. 20) or after reflection of the two source beams at the same interface (second term in the sum). Both contributions propagate indeed with phase mismatch equal to $\pm\Delta k_{z,T}^{[2]}$. Selecting a single dominant process is less straightforward here than in transmission because the two leading contributions in Eq. 20 have orders of magnitude closer to each other. In addition, in practical applications, SFG emitted in reflection may compete with a third process, namely the direct process generated in transmission, going out of the system then back reflected into the system from medium [3] by the presence of a reflector in the experimental set-up. In particular, this third process may not be neglected when {23} transmission coefficients are favourable and the reflector has a high efficiency like a metal, which is typically the case in an electrochemical set-up using p-polarized light with incidences close to the Brewster angles.[45]

In all cases, the leading contributions stem from a combination of Eq. 19 and 17, all bearing a common amplitude dependence on $\Delta k_{z,T}^{[2]}$ through the sinc function. We may wrap the various components into the dressed susceptibility and concentrate on the dependence of the emitted signals on the argument of the sinc function, as is usually done as soon as phase matching is under consideration.[46]

E. Macroscopic layers in transmission

1. Three-layer system

When thickness of the bulk layer is large, and all the more when it becomes macroscopic, we have seen in Ref. 24 and 25 that the influence of the beams reflected inside this layer

decreases. For a macroscopic layer emitting in transmission (Eq. 18), one may expect that mostly unreflected beams, with Fresnel factors weighted by $A_\alpha^T A_\beta A_\gamma$ alone, interact inside the bulk and that the direct SFG process naturally dominates the nonlinear response. There is therefore no ambiguity in considering that the SFG response in transmission is essentially driven by the direct term. We note that neglecting the Fabry-Pérot effect inside a macroscopic film leads to identify coefficients A_{α_i} to Fresnel factors of the two-layer model inside layer [2] (2L–), leading to

$$\chi^{(2)}_{eff,T} \approx D\,\mathrm{sinc}\left(\frac{\Delta k^{[2]}_{z,T} D}{2}\right) e^{i\frac{\beta_1+\beta_2-\beta_3}{2}} \sum_{\alpha\beta\gamma} e^{[3]}_\alpha e^{[1]}_\beta e^{[1]}_\gamma F^{2L-,T}_\alpha F^{2L-}_\beta F^{2L-}_\gamma \chi^{(2)}_{B,\,\alpha\beta\gamma} \qquad (21)$$

Formally, the transmitted bulk SFG process in the macroscopic layer corresponds to the downward propagation of the incoming beams in the upper 2L-system {1,2} down to the middle of layer [2], as shown by the explicit phase $(\beta_1+\beta_2)/2$, where a second order polarization sheet is created by a surface nonlinear susceptibility equal to $D\,\mathrm{sinc}\left(\frac{\Delta k^{[2]}_{z,T} D}{2}\right)\boldsymbol{\chi}^{(2)}_B$, which generates a downward beam at the SFG frequency propagating forward (hence the phase $-\beta_3/2$) in the lower 2L-system {2,3}. An alternate interpretation of the generation process in such a thick layer is provided below in Part IV A.

2. N-layer system

We have seen[25] that the Fresnel factors applying to the bulk of layer [k] in the N-layer system simplify when this layer becomes macroscopic. More precisely, they may be decomposed as a product between the transmission of subsystem {1;k} (called $F^{\{1;k\}-}$) and the Fresnel factor in layer [k] as belonging to the {k;N} subsystem. For SFG measured in transmission, keeping only the direct product proportional to $A_\alpha^T A_\beta A_\gamma$ in Eq. 18 is equivalent for the incoming beams (resp. the transmitted SFG beam) to neglecting reflection at the {k} (resp. {k-1}) interface, as $r^{k,k+1}_{s/p}$ (resp. $r^{k,k-1}_{s/p}$) drives the B_β and B_γ (resp. B_α) contributions in Eq. A18-A20 (resp. Eq. A24-A26). It has been shown[25] that, in this particular case, Fresnel factors in layer [k] reduce to $F^{\{1;k\}-}$ (resp. $F^{\{k;N\}-}$) alone multiplied by phase factor $e^{i\beta^{[k]}(z_0)}$ (resp. $e^{-i\beta^{[k]}(z_0)}$) quantifying the dephasing induced by propagation in layer [k]. We therefore identify $A_{\beta/\gamma}$ to $F^{\{1;k\}-}_{\beta/\gamma}$, and A^T_α to $F^{\{N;k\}-}_\alpha$. Integration over z_0 leads to

$$\chi^{(2)}_{eff,T} \approx d^{[k]}\,\mathrm{sinc}\left(\frac{\Delta k^{[k]}_{z,T} d^{[k]}}{2}\right) e^{i\frac{\beta^{[k]}_1+\beta^{[k]}_2-\beta^{[k]}_3}{2}} \sum_{\alpha\beta\gamma} e^{[3]}_\alpha e^{[1]}_\beta e^{[1]}_\gamma F^{\{N;k\}-}_\alpha F^{\{1;k\}-}_\beta F^{\{1;k\}-}_\gamma \chi^{(2)}_{B,\,\alpha\beta\gamma} \qquad (22)$$

This shows that, as in the three layer case, SFG emitted in transmission by a macroscopic layer [k] is equivalent to a split process involving (i) propagation of both incoming beams to the middle of layer [k] (through the "upper" {1;k} subsystem with full account of Fabry-Pérot interference effects); (ii) generation of an equivalent surface nonlinear polarization and SFG emission (equivalent surface nonlinear susceptibility $d^{[k]}\,\mathrm{sinc}\left(\frac{\Delta k_{z,T}^{[k]} d^{[k]}}{2}\right)\boldsymbol{\chi}_B^{(2)}$); (iii) propagation of SFG radiation through the second half of layer [k] then across the "lower" {k;N} subsystem, finally leading to far field emission in medium [N].

Having established the rules governing the evolution of the bulk nonlinear response as a function of experimental parameters in various film configurations, in particular as for its leading terms, we may now consider how bulk contribution may impact on experimental spectra of transparent centrosymmetric materials, and how interference fringes help identify bulk from surface response.

IV. INTERFERENCE FRINGES FROM A MACROSCOPIC LAYER

A. Principles

Without loss of generality, we consider in the following the SFG emitted in transmission by a macroscopic bulk layer in the three layer system as a simplified representative of the general N-layer situation. We note that it may be seen as a generalization to three-wave mixing of the SHG process used to measure the bulk nonlinearities with the help of the so-called Maker fringes,[47] for which the essential features are indeed described for an arbitrary angle of incidence by the "direct" process, and account of the internal reflections appear in most cases as a higher order correction.[48] We rewrite Eq. 21 as

$$\chi_{eff,T}^{(2)} = \chi_{eff,B}^{(2)} \frac{i}{\Delta k_{z,T}^{[2]}} \left[1 - e^{i(\Delta k_{z,T}^{[2]})D}\right]. \tag{23}$$

This expression shows that the bulk SFG emission in transmission geometry is also equivalent to the SFG intensity generated by two surface nonlinear susceptibilities set in medium [2], one equal to $i\boldsymbol{\chi}_B^{(2)}/\Delta k_{z,T}^{[2]}$ located at the entrance interface $z_0 = 0^-$ and the second one, with opposite sign, at the exit interface $z_0 = D^+$, hence its phase factor. The total emitted

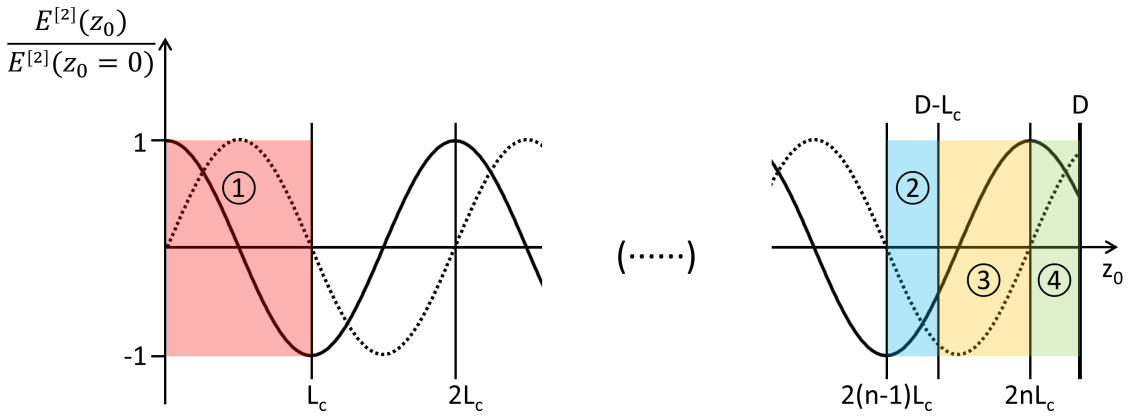

FIG. 2. Evolution of the complex amplitude of the SFG electric field along propagation in the bulk, normalized by its value at the entrance. Plain line: real part, dotted line: imaginary part.

intensity then follows the classical phase matching curve:[32,49]

$$I(\omega_3) \propto \left(\frac{\omega_3}{\cos\theta_3^{[3]}}\right)^2 \left|\chi^{(2)}_{eff,B}\right|^2 \frac{\sin^2\left(\Delta k^{[2]}_{z,T} D/2\right)}{\left(\Delta k^{[2]}_{z,T}\right)^2}, \tag{24}$$

with an alternate increase and decrease of the outgoing intensity when D grows, reaching maximal and zero intensities for $D = (2n+1)L_c$ and $D = 2nL_c$, respectively, where the coherence length L_c is defined by $L_c = \pi/|\Delta k^{[2]}_{z,T}|$. This results in fringes with period linked to the ratio L_c/D. These fringes vary dramatically with the value of $\Delta k^{[2]}_{z,T}$, which happens to be calculated as the difference between two almost equal quantities ($k^{[2]}_{1,z} + k^{[2]}_{2,z}$ and $k^{[2]}_{3,z}$). Its small value is therefore very sensitive to the differences between the SFG refractive index on one side, and the visible and IR indices on the other side, to an accuracy in the 10^{-4} range,[48] as is rather common when transmission phase matching is involved.[50]

The origin of the sign change of the effective surface susceptibility at $z_0 = D^+$ may be understood graphically. On Fig. 2 is shown the evolution of the complex amplitude of the SFG electric field inside bulk layer [2] as a function of z_0. The total emitted field is the integral of this local field over the whole layer from $z_0 = 0$ to $z_0 = D$. We see that the field changes sign after travelling over L_c, and consequently integration over any interval with length $2L_c$ vanishes. Integration over the whole bulk therefore boils down to the integration over zone 4 (called I_4), i.e. after removing an even number of coherence lengths. We may add zones 1, 2 and 3 to the integration ($I_1 + I_{\{2+3\}} = 0$) without changing the result. Considering

that integral I_2 is opposite to integral I_4, we have

$$I_4 = \frac{1}{2}\left[I_1 + I_{\{3+4\}}\right] = \frac{1}{2}\left[I_1 + e^{i(\Delta k_{z,T}^2)D}\, I_{\{2+3\}}\right] \quad (25)$$

$$= \frac{1}{2} I_1 \left[1 - e^{i(\Delta k_{z,T}^2)D}\right] \quad (26)$$

Eq. 26 allows to recover Eq. 23, whereas Eq. 25 shows that the full bulk contribution sums up a L_c-long contribution I_1 from the entrance surface, and a second L_c-long contribution $I_{\{3+4\}}$ from the exit side, shifted by $e^{i(\Delta k_{z,T}^{[2]})D}$ and opposite in sign as $I_{\{2+3\}} = -I_1$. As for the amplitude $i\chi_{eff,B}^{(2)}/\Delta k_{z,T}^{[2]}$ of this bulk contribution, it may also be understood graphically. Inspecting the curves on Fig. 2 shows indeed that integration over zone 1 leads to I_1 having a vanishing real part and a positive imaginary part proportional to L_c. This explains why it reduces to an equivalent imaginary surface contribution located at $z_0 = 0$, with an amplitude proportional to the bulk susceptibility $\chi_{eff,B}^{(2)}$ by a factor $I_1/2$ with $I_1 = \int_0^{L_c} e^{i\pi z_0/L_c} dz_0 = iL_c/\pi \int_0^{\pi} \sin\eta \, d\eta = 2i/\Delta k_{z,T}^{[2]}$.

Maker fringes make use of the SHG phase mismatch by observing oscillations in the output SHG signal when the effective thickness of the sample is varied by changing its tilt angle with respect to the fixed incoming beam.[47,51] The fringes, and in particular the positions of their minima, allow precise measurement of the nonlinear coefficients by comparison to a known material, on the condition that the phase mismatch is precisely known. This implies a knowledge of the dispersion of the refractive index within 0.1% or less. When this cannot be achieved, a fit of experimental data provides the required phase mismatch, to the expenses of nonlinear coefficient accuracy.[48] Eq. 24 shows that, when IR-visible SFG is involved instead of SHG, there is another way to get the oscillation fringes: modulation of $\Delta k_{z,T}^{[2]}$ may stem from wavelength tuning rather than from angle tuning. The phase mismatch varies indeed when the infrared wavenumber (ω_2) is tuned by the experimenter, which is rather easily achieved on a vibrational SFG set-up. The great advantage in this case is that one keeps all angles of incidence fixed, so that only the phase mismatch, and to a lower extent factor $(\omega_3)^2$, varies with ω_2. Considering the narrow range of variation for ω_3 and the usually very stable values of the refractive indices of materials over an infrared scan out of the phonon excitation domain, one may also consider $\cos\theta_3$ in all media and all Fresnel factors as essentially constant when scanning the infrared. All the information about the fringes therefore lies in Eq 24, in particular their period. Conversely, in a Maker-type experiment, the envelope of the fringes, responsible for the positions of the maxima, is a function of

several factors all depending on the tuned angle of incidence,[48] which have to be carefully taken into account. Finally, we may fruitfully combine these results with those describing the interference process between surface SFG produced at the entrance and exit interfaces[24,25] of the bulk layer. By modulating its thickness, it seems conceivable to efficiently separate surface and bulk SFG contributions of such a layer embedded in a multilayer system.

B. Low dispersion materials

In a material where dispersion is low, we may neglect the changes in $n_2^{[2]}$, $n_3^{[2]}$ and $\theta_3^{[2]}$ when ω_2 is tuned. With fixed angles of incidence, the phase mismatch is separated into a sum of a ω_1-term and a ω_2-term, becoming a linear function of ω_2, as

$$c|\Delta k_{z,T}^{[2]}| = \omega_2(n_3^{[2]}\cos\theta_3^{[2]} - n_2^{[2]}\cos\theta_2^{[2]}) + \omega_1(n_3^{[2]}\cos\theta_3^{[2]} - n_1^{[2]}\cos\theta_1^{[2]}). \tag{27}$$

This means that we may directly draw the transmitted SFG intensity as a function of ω_2 to visualize the fringes. In order to have a better understanding of the importance of the various parameters involved, we note that, for ω_2 in the infrared and ω_1 in the visible, we have ω_3 close to ω_1, leading to $n_3^{[2]} \approx n_1^{[2]}$ and $\theta_3^{[2]} \approx \theta_1^{[2]}$. Using $\cos\theta_1^{[2]} \approx \cos\theta_3^{[2]} - (\theta_1^{[2]} - \theta_3^{[2]})\sin\theta_3^{[2]}$ and $\sin\theta_1^{[2]} \approx \sin\theta_3^{[2]} + (\theta_1^{[2]} - \theta_3^{[2]})\cos\theta_3^{[2]}$ to rearrange Eq. A2 and 27, we may rewrite the phase mismatch into

$$c|\Delta k_{z,T}^{[2]}| \approx \frac{1}{\cos\theta_3^{[2]}}\left\{\omega_2\left[n_3^{[2]} - n_2^{[2]}\cos(\theta_2^{[2]} - \theta_3^{[2]})\right] + \omega_1(n_3^{[2]} - n_1^{[2]})\right\}. \tag{28}$$

Qualitatively, and quantitatively within a few percents in most usual experimental configurations (e.g. $|\theta_2^{[2]} - \theta_3^{[2]}| < 20°$), the evolution of $\Delta k_{z,T}^{[2]}$ as a function of ω_2 is essentially linear, with a slope proportional to the difference in the refractive indices at the SFG and infrared energies, and a constant shift proportional to ω_1 and to the difference in the refractive indices at the SFG and visible energies. The overall scaling factor, $\cos\theta_3^{[2]}$, is mainly driven by the value of $\theta_1^{[1]}$ and $n_3^{[2]}$. It is therefore possible to independently tune the slope and the constant shift by playing separately with two properties of the visible beam: visible color ω_1 and visible angle of incidence $\theta_1^{[1]}$. From Eq. 28, plotting the fringes using Eq 24 while tuning the infrared gives birth to a period T_σ given, when expressed in infrared wavenumbers $\sigma_2 = \omega_2/2\pi c = 1/\lambda_2$, by

$$T_\sigma \approx \frac{1}{D}\frac{\cos\theta_3^{[2]}}{n_3^{[2]} - n_2^{[2]}\cos(\theta_2^{[2]} - \theta_3^{[2]})} \tag{29}$$

For a macroscopic film ($D \gg \lambda_2$, leading to a thickness from 100µm to the few centimeter range), $1/D$ lies between one hundred and a fraction of cm^{-1}. Including the correction factors in Eq. 29, in particular the denominator, shifts the period towards higher values. Observation of the fringes, that one may estimate as comfortable when the period lies in the 10 to 100 cm^{-1} range, relies thus on a balance between film thickness and material dispersion, to be adjusted by the experimenter: the more dispersive the material, the smaller the thickness.

C. High dispersion materials

In such materials, the variations of the indices and, to a lower extent, of the angles as a function of ω_2 for beams 2 and 3 in Eq. 27 and 28 cannot be neglected. As the differences in refractive indices modulate the ω_1 and ω_2-terms, their behaviours differ. For normal dispersion, $n_3^{[2]}$ increases with ω_2, leading to an increase in the ω_1-term. On the contrary, the increase in ω_2 may be compensated or amplified in the ω_2-term by the dispersion in the difference $n_3^{[2]} - n_2^{[2]}$ (as both $n_2^{[2]}$ and $n_3^{[2]}$ increase). As a consequence, the effective period of the fringes differs from the prediction of Eq. 29 and is not constant over the spectrum under the influence of both terms. In this case, plotting the fringe spectrum is still possible, but an accurate modeling becomes difficult because it relies on very small variations of the indices, which are hard to benchmark with high accuracy. When this cannot be achieved, an analysis is still possible using the low dispersion approximation to estimate the average period of the fringes.

D. Examples of experimental bulk SFG fringes

Bulk SFG is seldom considered experimentally for itself (with the notable exception of liquid bulks[11,52]), because the interest of the technique essentially lies in the spectroscopic analysis of very small amounts of matter at interfaces. In some cases, bulk SFG signals may however represent an additional experimental contribution disturbing or even overwhelming the response of the interface.[9,15] We present here several examples of bulk SFG signals which properties follow the principles described above. In particular, we focus on the bulk response of centrosymmetric materials transparent in the infrared and the visible ranges

(diamond, CaF_2, BaF_2, silica glass) for which long range propagation of the three beams can be achieved. In principle, they should not generate any bulk SFG as a consequence of their symmetry properties and of the absence of phonon excitations by light in the probed infrared ranges. As a consequence, these materials are conveniently used as substrates to support adsorbed molecular monolayers, and as windows or prisms closing experimental cells for controlled chemical conditions (gas phase, liquid interfaces, electrodes under electrochemical control) as they let incoming and outgoing light beams pass through for SFG spectroscopy. It may seem surprising that such materials, designed as SFG-free, may be used precisely to study bulk SFG response. Generation of bulk Sum-Frequency intensity from these materials may have several origins: (i) a weak symmetry-allowed quadrupolar contribution may become measurable for a thick material because of the amount of matter probed; (ii) some defects or inclusions in their crystal structure may alter their local symmetry properties and create a small density of bulk SFG-active centers; (iii) the use of intense and sometimes highly focused laser beams may dynamically disturb the ideal centrosymmetric crystal structure through heat exchange[53] or even local damage over the laser overlapping zone, making them slightly SFG-active. It is in fact important to characterize the conditions leading to such a "forbidden" SFG emission in order to avoid artefactual signals from these materials to compete with the sought-after molecular signatures.

We have used an experimental SFG setup with the following properties. The visible source stems from a Nd:YVO_4 laser (7.5 ps, 62.5 MHz) which, after temporal shaping in 2 μs long trains at 25 Hz followed by amplification and frequency tripling, synchronously pumps a visible OPO to generate tunable visible colors. The infrared source used here was the CLIO free electron laser, providing $\sim$1ps pulses with the same time structure as the visible OPO, widely tunable in the infrared range. The two lasers are focused, temporally synchronized and geometrically overlapped on the sample to generate SFG photons in the ppp polarization configuration, measured either in transmission or in reflection after spatial and frequency filtering through a Notch filter and a double grating monochromator (Acton Trivista).

As a example of the phase mismatch interference fringes, we first consider a CVD diamond window (511μm thick, Diamond Materials) in the far infrared range (250-900cm^{-1}). The visible wavelength was set at 532nm (angle of incidence 38.8°), and we used KRS-5 optical parts for the IR line (angle of incidence 55°). In Fig. 3, we present the interference fringes

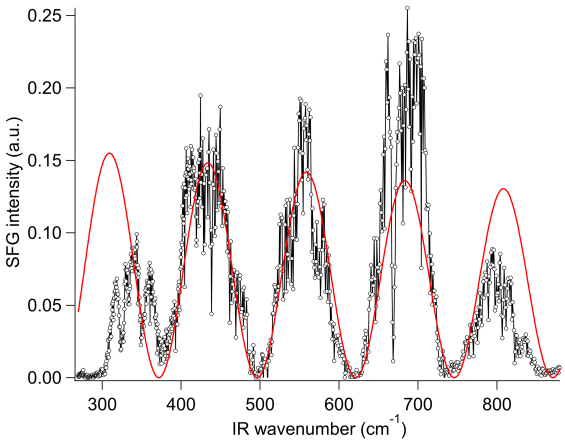

FIG. 3. SFG interference fringes of a 511μm thick CVD diamond window. Open dots are experimental points, red line a fit according to Eq. 24 as explained in the text.

measured in the transmission geometry. The full IR interval has been scanned in several overlapping spectra, put together to reconstruct the complete spectrum. Various absorption bands from water and carbon dioxide are used to check the calibration of the IR wavelength. The measured signals are rather high even though the symmetry of diamond should prevent bulk SFG to be measured, as the phonons are not infrared-active. The signal may thus be referred to as "nonresonant", stemming from quadrupolar interaction or local disturbance of the perfect diamond crystal structure as explained above. As a corollary, contrary to what could be expected, such a diamond window cannot be considered an appropriate material to act as the entrance window of an experimental cell in the far infrared.

The period is measured as approximately 120cm^{-1}, which is far too much for a pure Fabry-Pérot effect. The dispersion in refractive indices for the CVD diamond used here is not known with a great accuracy, so we use the low dispersion approximation. Considering Eq. 29 with $\theta_2^{[2]} - \theta_3^{[2]} \sim 6°$, the experimental period corresponds to a calculated difference of 0.14 between the SFG and IR indices of refraction. Tabulated refractive indices in the visible (around 2.42-2.43) and infrared ranges (around 2.36-2.38) for natural and CVD diamond favor a value around 0.06, which does not fit.[54–57] However, the optical properties of such a synthetic material strongly depend on its preparation conditions and local structure and, as already mentioned, the period of the fringes is extremely sensitive to small changes in the refractive indices. The transmission curves provided by the manufacturer of our diamond window show peculiar properties which differ from usual diamond materials. First,

transmission in the infrared reaches 75%, far above the predicted limit for Fresnel losses,[58] showing that the refractive index in this region is lower than the theoretical values. Values as low as $n_2^{[2]} = 2.29$ in the infrared have for example been reported.[59] Second, transmittivity varies a lot in the visible range, even between visible and SFG frequencies: the values (68% and 67%, respectively), correspond to refractive indices around 2.44 and 2.48, respectively.

As an illustration, we plot on Fig. 3 the fringes calculated with D=511μm, $n_1^{[2]} = 2.4397$, $n_2^{[2]} = 2.3420$ and $n_3^{[2]} = 2.4820$. We see that the essence of the oscillations is recovered, whereas the theoretical amplitudes are more regular than the experimental ones. This may be due to several experimental effects: stability and pulse to pulse reproducibility of the IR power during the scan of the IR wavelength, jitter on the delay between the visible and IR pulses, full spectrum split into several experimental scans. In particular, we note that the low energy peak seems to shift off the regular spacing of the other maxima. This low energy part of the spectrum is perturbed by the transparency edge of KRS-5 material and by the bandwith of the Notch filter in the detection line, which in fact remove most SFG photons produced below 300cm^{-1}. The true peak position at low energy may therefore lie further to the lower frequency side of the spectrum. On the theoretical point of view, discrepancies between data points and model may be due to the neglect of some contributions among the eight terms detailed in Part III A, in particular the second term in Eq. 18. We should also consider that the infrared wavenumbers in this experiment are very small, so the second lowest term in the $\Delta k^{[2]}_{z,\{\pm\pm\pm\}}$ series, namely $\Delta k^{[2]}_{z,-+-} = [k^{[2]}_{1,z} - k^{[2]}_{2,z} - k^{[2]}_{3,z}]$ has a value only between 2.4 and 5 times higher than $\Delta k^{[2]}_{z,T}$, so its intensity (Eq. 24) scales like 5.8 to 25 that of the leading term. Of course, its influence is lowered because, in transmission geometry, it also encompasses reflection coefficients at the boundaries, which is not the case of the direct leading term. Finally, we have not taken into account the unknown dispersion of the refractive indices from point to point (for ω_2 and ω_3), which may distort the calculated fringes with respect to the experimental ones.

The existence of these experimental phase mismatch fringes for a centrosymmetric material like diamond, which in principle should not show any measurable bulk SFG signal, leads us to wonder whether this phenomenon could have been observed in the past from wafers or windows. Scanning the literature, we have found two striking examples of experimental data which seem compatible with such interference fringes. In spite of its centrosymmetry, glass is known to produce bulk SHG in some conditions,[60] with bulk contributions of the same

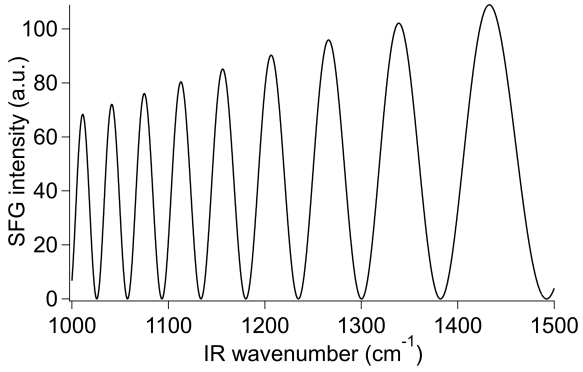

FIG. 4. Simulated SFG interference fringes of a 2mm thick CaF_2 window.

order of magnitude as the surface ones,[61,62] as was also observed by SFG in transmission.[23] In a series of papers, a group from Pennsylvania State University has studied the SFG response of soda lime glass wafers.[63–65] In these papers, they observed oscillations in the SFG response in the 3000–4000cm^{-1}, which were attributed to OH stretching modes.[64] Five regularly spaced maxima were measured for a 1mm thick glass wafer, and only three for a 0.7mm thick wafer, with the SFG intensity reaching zero between all peaks. Here we propose an alternate explanation, namely phase mismatch fringes arising from bulk SFG production in transmission and back-reflected to the SFG detector. As for the diamond window, the optical properties of float glass (refractive index and dispersion) are not accurately known as they depend on glass composition. We therefore rely on the low dispersion approximation to assess the likelihood of this hypothesis. Using standard soda lime glass values[66] for the indices of refraction in Eq. 29, we obtain for the period of the fringes $T_\sigma =$ 186.1cm^{-1} at 3500cm^{-1} for a thickness of 1mm. The experimental spacings between maxima are equal to 212, 160, 176 and 192cm^{-1}, these values match the predicted period. More interestingly, the spacings between experimental maxima increase when the wafer thickness decreases to 0.7mm, reaching values 272 and 280cm^{-1}. In these conditions, the predicted period for the fringes increases to 265.9cm^{-1}, close to the experimental value. The fact that the experimental period seems indeed inversely proportional to the thickness of the wafer is a good indication that the bulk nature of the signals, i.e. phase mismatch fringes, cannot be discarded.

In the second example, a CaF_2 window was used to close a spectro-electrochemical cell to let all laser beams reach the platinum electrode surface to perform SFG *in situ*.[45] Here, no

less than nine clear maxima were measured in the 1000–1500cm^{-1} range, regularly spaced, with a period increasing with the infrared wavenumber. Some other features were more difficult to distinguish in the spectra. Our hypothesis is again that these maxima, rather than originating in molecular vibrations, may stem from the phase mismatch fringes in transmission, this time probably back-reflected by the Pt electrode itself. The interesting point in this study is that the material (CaF_2 crystal) is this time very well known and its optical properties tabulated with great accuracy using a Sellmeier equation.[67] It becomes therefore possible to simulate these fringes using the exact dispersion of the refractive index and compare their positions to the experimental ones. We show in Fig. 4 the predicted fringe spectrum for a 2mm CaF_2 window using Eq. 24 and 27. The spectrum strikingly resembles the original experimental one, with maxima located at 1011.2, 1041.4, 1075.0, 1113.0, 1156.3, 1206.5, 1266.1, 1338.8 and 1432.7cm^{-1}, closely following the original values (1030, 1056, 1084, 1122, 1168, 1214, 1270, 1330/1348 and 1432cm^{-1}) within an acceptable error on the exact positions of the experimental peaks. We have checked that, in this region, $\Delta k^{[2]}_{z,-+-}$ has a value between 11 and 22 times higher than $\Delta k^{[2]}_{z,T}$, so its intensity (Eq. 24) is of the order of 1% (and below) that of the leading term.

In the two previous examples, we do not claim that the original interpretations in terms of OH stretches and adsorbate vibration modes, respectively, are wrong. We rather suggest that an alternate explanation should be considered in terms of phase mismatch fringes, and that this deserves at least further experimental analysis in order to solve this open question. It is also possible that both types of signals are superimposed on the experimental spectra. We understand that the authors of these studies were aware of the striking regularity of their peaks, and that they have provided additional experimental evidence in order to discard the possibility of an artefact. In the soda lime glass case,[64] an index-matching liquid was added to the experimental cell to remove reflected beams, and no difference was observed. This indeed is a good way to get rid of interference patterns due to Fabry-Pérot effects in the wafer. However, our alternate explanation involves bulk SFG produced by a $\chi_{eff,B}$ characteristic of the glass wafer along the course of the three beams, with a period linked to the thickness of the wafer. When the index-matching liquid is added, it generates no bulk SFG, so the signal, still produced inside glass alone in transmission following the direct process, remains unchanged. In the second example, the experiment was repeated in the absence of the molecular species, and the observed peaks disappeared.[45] This observation is

more difficult to account for, but could be due to a change in beam alignment and overlap, concentrating on the high peak at 1408cm^{-1}, to the expenses of the observation of the fringes. On some spectra, it is possible to see that the fringes sometimes appear at the very limit of detection (e.g. spectrum with applied potential 0.9V in Figure 5). Finally, it could have been assumed that the fringes arise from surface terms instead of bulk. More precisely, interference between SFG surface contributions from the entrance and exit planes could give rise to fringes modulated by phase mismatches. Going back to the three-layer equations governing the phase evolution of these two contributions[24] shows that, this time, the eight terms from Eq. 6 and 7 coexist in the final response, each one with its own fringe period. Contrary to the bulk case, there is no selection of a dominant process through the value of denominator $\Delta k_{z,T}^{[2]}$. In the reflection geometry in particular, the direct reflected process is expected to be high, exhibiting a much shorter period for the fringes. There is no experimental evidence of such a signal (neither in the results above nor in our reflection measurements of the diamond window), which is a clear signature of the bulk origin for the fringes.

V. ALTERNATE ORIGIN OF PSEUDO-RESONANT BULK SFG RESPONSE

This work on CaF_2 (Ref. 45) is very interesting also because the experimental spectra therein show another type of contribution from the CaF_2 window, apart from the phase mismatch fringes, namely the giant peak at 1408cm^{-1}. This peak has been observed by several groups in the world[68] but most published data do not mention its existence because no explanation of its origin has ever been given.[69] In order to determine the source of this peculiar feature, we have recorded dedicated spectra using SFG and DFG spectroscopies with a tunable visible color. A CaF_2 equilateral prism was used in air in total internal reflection configuration, with angles of incidence at the entrance plane equal to +5.0° for the infrared beam and -5.3° for the visible beam, respectively. The CLIO free electron laser was tuned in the 1100–1500cm^{-1} range, and the visible color set to five values: 442nm, 488nm, 532nm, 568nm and 594nm. As expected, a very intense peak was seen on all SFG and DFG spectra (Fig. 5). Their profiles were nicely fit with a gaussian curve to determine the positions of their maxima. From these spectra and the literature, we can observe the following facts:

(i) the peak is observed in different configurations: a flat window in Ref. 45, a prism in total reflection, and a prism in contact with water[69] (i.e. without total reflection); (ii) the SFG peak position at 532nm differs between the flat window (1408cm^{-1}) and the prism (1352cm^{-1}); (iii) the peak position varies when the visible color is tuned, and when SFG is switched to DFG; (iv) the peaks were equally measured with the free electron laser (high peak power, pulse duration ∼1ps) and a tabletop OPO (low peak power, pulse duration 25ps) as the IR source; (v) the peaks seem broader in Fig. 5 than in Ref. 45; (vi) peak positions do not depend on the sample thickness, contrary to the phase mismatch fringes. From these facts, we know that this signal is not IR-resonant with a conventional vibrational feature (e.g. phonon), and not related to the total reflection phenomenon. In addition, the visible beam properties are clearly involved, either energy or wavevector. Discrepancies in vibrational frequencies as experimentally measured by SFG and DFG have recently been reported.[70] This phenomenon was explained by an asymmetric temporal overlap between IR vibrational polarization and visible pulse as a consequence of frequency dispersion and distortion of the visible pulse. Such a phenomenon is thus specific to molecular vibrations and short pulse (i.e. broadband) nonlinear spectroscopy, which is not relevant here.

Here we propose the following interpretation. The source of the signal is still bulk SFG produced in the forward direction along the course of the three beams and detected in reflection geometry. From the analysis of the phase mismatch fringes, we know that the SFG intensity emitted in the forward direction depends very precisely on the value of $\Delta k_{z,T}^{[2]} = k_{1,z}^{[2]} + k_{2,z}^{[2]} - k_{3,z}^{[2]}$. The three beams involved in the SFG process have a finite duration, which means that they carry a distribution of frequencies ($\widetilde{\omega}_i$) around their central frequency (ω_i). For these non-central frequencies, the values of $\widetilde{k}_{i,z}^{[2]}$ differ from the central $k_{i,z}^{[2]}$, i.e. it is not a constant over the whole components of the laser pulse. As a consequence, the phase mismatch $\Delta k_{z,T}^{[2]}$ is neither a constant for the whole SFG process, which involves all the combinations of frequencies $\widetilde{\omega}_3 = \widetilde{\omega}_1 + \widetilde{\omega}_2$. Several components with different $\Delta\widetilde{k}_{z,T}^{[2]}$ participate in the phase matching process and, for example, when $\Delta k_{z,T}^{[2]} D/2$ corresponds exactly to a maximum, the neighbouring $\Delta\widetilde{k}_{z,T}^{[2]} D/2$ don't. The full process is thus the sum of elementary processes, all of them slightly out of phase with respect to the others. As phase coherence is not maintained over the whole pulses, the maxima measured in the fringe spectra do not imply the total intensity of light interacting in phase. We have seen in the previous Part that a small variation of $\Delta k_{z,T}^{[2]}$ leads to a dramatic change in the

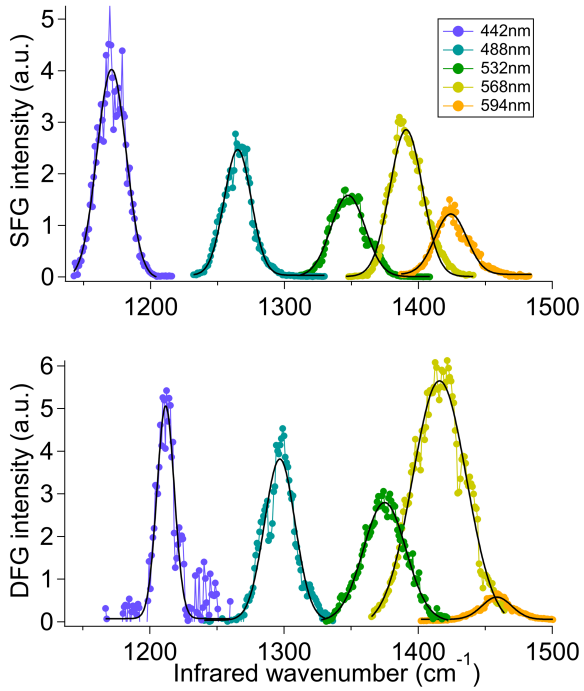

FIG. 5. SFG (top) and DFG (bottom) spectra recorded in internal reflection inside a CaF_2 prism. Five visible colors were used in each panel. Peak positions are determined by a Gaussian fit (black lines).

fringes. In fact, in the analysis of the fringes in Fig. 3 and 4, the maxima were observed for $\Delta k^{[2]}_{z,T} D = 2n\pi$, with n varying between 44 and 49 for diamond, 30 and 39 for CaF_2, respectively. A 1% change in $\Delta k^{[2]}_{z,T}$ represents more than 30% change in phase for a single beam, which accumulates over the three beams.

In order to quantify this dephasing process, we may write at first order[71]

$$\Delta \widetilde{k}^{[2]}_{z,T} \approx \Delta k^{[2]}_{z,T} + \sum_{i=1}^{3} (\widetilde{\omega}_i - \omega_i) \left(\frac{\partial \Delta k^{[2]}_{z,T}}{\partial \widetilde{\omega}_i} \right)_{\widetilde{\omega}_i = \omega_i} \tag{30}$$

We see that, if

$$\sum_{i=1}^{3} \omega_i \left(\frac{\partial \Delta k^{[2]}_{z,T}}{\partial \widetilde{\omega}_i} \right)_{\widetilde{\omega}_i = \omega_i} = 0, \tag{31}$$

the quantity $\Delta \widetilde{k}^{[2]}_{z,T}$ will remain almost equal to $\Delta k^{[2]}_{z,T}$ for all frequencies close to ω_i. This means that the overall phase of the SFG process induced by the phase mismatch remains almost constant over the whole pulses when Eq. 31 is fulfilled, and SFG is coherently produced by all frequencies composing the pulses, leading to an enhancement of the SFG output. In a

simple view, we consider a frequency $\widetilde{\omega}_1$ scanning the frequencies carried by the first pulse, and $\widetilde{\omega}_2$ scanning the second pulse, so that $(\widetilde{\omega}_1 - \omega_1)/\omega_1 = (\widetilde{\omega}_2 - \omega_2)/\omega_2$. In this case, this quantity $(\widetilde{\omega}_3 - \omega_3)/\omega_3$ is equal to the two others for the SFG pulse too and ω_3 identically scans the SFG pulse, so that $(\widetilde{\omega}_i - \omega_i)/\omega_i$ is a constant quantity of the process. Plugging this into Eq. 30, we get

$$\Delta\widetilde{k}_{z,T}^{[2]} \approx \Delta k_{z,T}^{[2]} + \frac{\widetilde{\omega}_i - \omega_i}{\omega_i} \sum_{i=1}^{3} \omega_i \left(\frac{\partial \Delta k_{z,T}^{[2]}}{\partial \widetilde{\omega}_i} \right)_{\widetilde{\omega}_i = \omega_i} \tag{32}$$

and conditions expressed by Eq. 31 leads to the equality between $\Delta\widetilde{k}_{z,T}^{[2]}$ and $\Delta k_{z,T}^{[2]}$, ensuring the phase coherence for all these elementary processes. This equation thus establishes a "phase mismatch resonance condition" of the bulk SFG process over the frequency distributions inside the three pulses. The experimental phenomenon described in Fig. 5 does not originate in a vibrational or electronic resonant transition of the sample, as is usually observed by SFG spectroscopy. Still, it consists of a giant increase in experimental intensity, peaking at one specific frequency in the spectra, with a finite width. As we shall see below, it follows in addition the phase mismatch resonance condition as a function of beam frequencies. Having all characteristics of a true resonant process, we dub it as "pseudo-resonant" in the following to avoid any ambiguity. From the definition of $\Delta k_{z,T}^{[2]}$, we have

$$c \left(\frac{\partial \Delta k_{z,T}^{[2]}}{\partial \widetilde{\omega}_i} \right)_{\widetilde{\omega}_i = \omega_i} = \varepsilon_i \left(\frac{\partial n_i^{[2]}}{\partial \omega_i} \omega_i \cos\theta_i^{[2]} + n_i^{[2]} \cos\theta_i^{[2]} - n_i^{[2]} \omega_i \sin\theta_i^{[2]} \frac{\partial \theta_i^{[2]}}{\partial \omega_i} \right) \tag{33}$$

where ε_i=1 for i=1, 2 and ε_3=-1, and $\left(\frac{\partial}{\partial \widetilde{\omega}_i} \right)_{\widetilde{\omega}_i = \omega_i}$ is written $\frac{\partial}{\partial \omega_i}$ for clarity. Differentiating Snell's law between media [1] and [2], we have, for a dispersionless medium [1],

$$\frac{\partial n_i^{[2]}}{\partial \omega_i} \sin\theta_i^{[2]} + n_i^{[2]} \frac{\partial \theta_i^{[2]}}{\partial \omega_i} \cos\theta_i^{[2]} = 0 \tag{34}$$

leading to

$$n_i^{[2]} \omega_i \frac{\partial \theta_i^{[2]}}{\partial \omega_i} = -\omega_i \frac{\partial n_i^{[2]}}{\partial \omega_i} \tan\theta_i^{[2]} \tag{35}$$

Finally, we obtain

$$c \left(\frac{\partial \Delta k_{z,T}^{[2]}}{\partial \widetilde{\omega}_i} \right)_{\widetilde{\omega}_i = \omega_i} = \varepsilon_i \left[n_{g,i}^{[2]} \cos\theta_i^{[2]} + (n_{g,i}^{[2]} - n_i^{[2]}) \sin\theta_i^{[2]} \tan\theta_i^{[2]} \right] \tag{36}$$

	Experimental	Calculated (corrected)	Calculated (uncorrected)	GVM only (corrected)	GVM only (uncorrected)
CaF_2 window	1408	1397.1	1322.6	993.4	954.9
BaF_2 (SFG)	1380.4	1382.1	854.5	-	-
BaF_2 (DFG)	1427.5	1428.8	883.4	-	-

TABLE I. Comparison between experimental and calculated peak positions (cm^{-1}) with and without correction of $n_g^{[2]}$ index for a CaF_2 window and a BaF_2 prism.

where $n_{g,i}^{[2]} = n_i^{[2]} + \omega_i \dfrac{\partial n_i^{[2]}}{\partial \omega_i}$ is the group velocity index. Eq. 31 is fulfilled when

$$\sum_{i=1}^{3} \varepsilon_i \, n_{g,i}^{[2]} \, \omega_i \, \cos\theta_i^{[2]} + \sum_{i=1}^{3} \varepsilon_i (n_{g,i}^{[2]} - n_i^{[2]}) \sin\theta_i^{[2]} \tan\theta_i^{[2]} = 0 \tag{37}$$

The first term is the group velocity mismatch (GVM) of the process,

$$\text{GVM} = \frac{1}{c} \left(n_{g,1}^{[2]} \, \omega_1 \, \cos\theta_1^{[2]} + \, n_{g,2}^{[2]} \, \omega_2 \, \cos\theta_2^{[2]} - \, n_{g,3}^{[2]} \, \omega_3 \, \cos\theta_3^{[2]} \right), \tag{38}$$

characterizing the phase differences induced by the propagation of the envelopes of the three laser pulses (whereas $\Delta k_{z,T}^{[2]}$ quantifies the phase velocity mismatch, accounting for the phase differences induced by the propagation of the light waves composing the laser pulses). This first term in Eq. 37 accounts for the refractive index dependence on the frequencies, whereas the second term may be seen as the contribution accounting for angular dependence on the frequencies. In a different formulation, the resonance condition may be written:

$$\left[n_{g,1}^{[2]} - n_1^{[2]} (\sin\theta_1^{[2]})^2 \right] \frac{\omega_1}{\cos\theta_1^{[2]}} + \left[n_{g,2}^{[2]} - n_2^{[2]} (\sin\theta_2^{[2]})^2 \right] \frac{\omega_2}{\cos\theta_2^{[2]}} = \left[n_{g,3}^{[2]} - n_3^{[2]} (\sin\theta_3^{[2]})^2 \right] \frac{\omega_3}{\cos\theta_3^{[2]}} \tag{39}$$

The group velocity mismatch has been thoroughly studied for optically active crystals because of its influence on the frequency generation processes in the bulk (e.g. SHG or OPO systems using BBO[72] and KTP[73,74] crystals). Here we propose a simplified, but operative, view of this phenomenon, which would require for a complete description a finer account of temporal and frequency structures of the pulses and of the coupled wave equations in the bulk.[75–77]

To check that this phenomenon is indeed the source of the experimental CaF_2 peak, we calculate the infrared wavenumber for which the resonance condition is fulfilled using

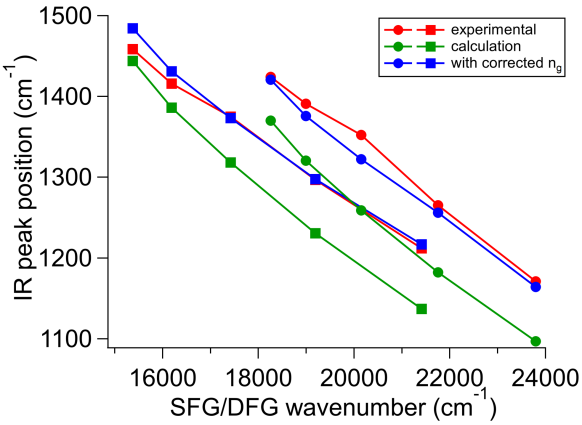

FIG. 6. Infrared resonance frequency (cm^{-1}) in the CaF_2 prism as a function of the experimental SFG (circles) and DFG (squares) wavenumber. Experimental values (red), calculated values according to Eq. 39 (green), calculated values after correction of group index $n_g^{[2]}$ (blue).

experimental parameters of Ref. 45 and Fig. 5. The group index is calculated from the derivative of the Sellmeier equation for the refractive index.[67] For DFG, Eq. 37 is modified using $\omega_3 = \omega_1 - \omega_2$ and ε_2=-1. The results for the CaF_2 prism are plotted in Fig. 6(A) as a function of the SFG and DFG experimental wavenumbers, respectively. Comparison between experimental values in red and calculated ones in green shows that the trend is nicely reproduced: the calculated resonance values lie a few tens of wavenumbers below the experimental ones, but the slopes as a function of the SFG and DFG energy is reproduced. Eq. 37 and 39 have succeeded in capturing the essential features of the phenomenon, linked to a group velocity phase matching of the SFG process during propagation in the bulk. This GVM is achieved for the envelopes of the laser pulses, traveling at the group velocity ($c/n_{g,i}^{[2]}$), rather than the individual light waves composing the pulses, traveling at the phase velocity ($c/n_i^{[2]}$). It is interesting to remind that, for a normally dispersive material, phase matching of the SFG process is impossible because of the continuous growth of the refractive index with the energies. However, the group index is not a monotonic function and often has a minimum in the transparency region for dielectric materials (because the refractive index varies more steeply at the edges of the transparency region, where resonant processes start increasing dispersion). For frequencies located on each side of this minimum, it may become possible to cancel the GVM term.

We have successfully reproduced the trends for the location of the CaF_2 giant peak, but

not exactly the values. This may be due to several reasons linked to various approximations in the derivation of the model: (i) only the first order in the derivative of $\Delta k^{[2]}_{z,T}$ has been taken into account. The second order, related to the group velocity dispersion (GVD) effect, may slightly shift the resonance wavenumber. GVD is usually considered for ultrashort pulses in the femtosecond range, which is not our case;[71] (ii) in a similar way, we have neglected the other $\Delta k^{[2]}_{z,\{\pm\pm\pm\}}$ terms from reflected beams and considered only the leading term $\Delta k^{[2]}_{z,T}$. Their contributions, even small, may alter the resonance condition; (iii) as for the phase mismatch fringes, the ω_2 value fulfilling the resonance condition is sensitive to the dispersion of the material to a great accuracy but, this time, dispersion involves both the refractive index and the group index. In the original publication, the Sellmeier equation was deduced to nicely fit the experimental data for the CaF_2 refractive index.[67] However, deriving this equation has not been originally designed to model the group index, which has not been cross-checked against experimental group index data. We may therefore expect a bigger error on the group index rather than on the refractive index. In order to estimate the amplitude of the error which could cause the discrepancies in Fig. 6(A), we have tried to slightly modify the values of $n^{[2]}_{g,i}$ in a coherent way over the visible and the infrared ranges. Adding to the group index a small corrective term in the 426–721nm range, quadratic as a function of visible wavenumbers (with a maximum of 1.4×10^{-3} at 535nm), together with a constant value of 0.01 in the IR range, leads to calculated positions of the pseudo-resonant peaks closer to the experimental values (blue points in Fig. 6). We see that very small changes in the group index suffice to match the experimental data points.

As was said before, the pseudo-resonant peaks in CaF_2 have also been observed in a flat window.[45] The experimental and predicted values appear in Table I. As above, the raw estimation is lower than the experimental one, but they closely match after the same correction in the CaF_2 group index as above is introduced. Interestingly, in this example we may check the essential contribution of the angular corrective term in Eq. 37. In the Table, we have shown the resonance frequencies calculated from the cancellation of the GVM term only, with and without correction of the group index. We see that the results (below 1000cm^{-1}) are far off the experimental value, proving that the angular term, complementary to GVM, is necessary to recover the experimental observation. In the prism configuration, this corrective term is very small indeed, as all angles are very close to zero, and its importance could not be tested. The observed pseudo-resonance is therefore not a pure GVM effect, rather

the proof of the existence of a stationary point in the $\Delta k_{z,T}^{[2]}$ function of ω_2. We may also note that the experimental peaks show up as Gaussian rather than Lorentzian profiles, and that they appears narrower in the window than in the prism. This may be accounted for by the origin of the pseudo-resonant process: in the laser pulses, the distribution of frequencies follows approximately a Gaussian profile. In addition, the peaks were measured in the prism using the CLIO free electron laser, for which the pulse length is around 25 times smaller than the OPO used for the window. The Gaussian frequency dispersion in the infrared pulse is therefore much smaller for the window than for the prism, which accounts for the differences in the experimental widths of the pseudo-resonant peaks.

In a last experiment, we have checked by SFG and DFG the existence of the same pseudo-resonance phenomenon in a BaF_2 prism using the same sources and the same incidence angles as the CaF_2 prism, with $\omega_{vis} = 532$nm. The experimental pseudo-resonant peaks, which positions are also given in Table I, appear close to the CaF_2 ones. However, the calculated positions lie very far from those, below 900cm^{-1}. A slightly bigger correction of the BaF_2 group index matches calculated and experimental values: 0.01 in the infrared, 0 for the SFG, 0.005 at 532nm and 0.01 for the DFG. This shows that the phenomenon should be universal, as it is not related to the nature of a specific material like calcium fluoride.

VI. CONCLUSION

Surface specificity represents the main asset of Sum-Frequency Generation, accounting for the stress put on the surface contributions in the literature. Bulk contributions on the other side can be considered as complementary or competing terms, and in worst cases as a nuisance interfering with the sought-after surface signals. Even if the theoretical framework used for the description of bulk terms appears sometimes different from the surface one, they both rely on the same underlying equations. Their intrinsic differences lie in the symmetries and the order of the optical processes involved (usually dipolar versus multipolar), but the surface contribution is originally a bulk one reduced to a very thin volume. We have shown that it is conversely possible to recover the bulk contribution from the surface formalism, even in the N-layer case. The advantage here is that the corpus of equations describing the surface contributions is well established and universally adopted by SFG users. It remains universal whatever the structure of the interface. For bulk terms, as for surface ones, all

the information about this structure is carried out by the Fresnel coefficients, including the phase terms. Phases are essential in the bulk because, as the bulk nonlinear susceptibility is supposed uniform over the whole material, all effects specifically induced by the bulk nature relate to beam propagation through the phases.

When considering the various beam reflections at each interface in the multilayer system, the number of beams involved in the SFG process becomes high, each one carrying its own phase. In some cases, the number of beams reduces or their dephasings may be neglected. This is in particular the case by construction for a semi-infinite bulk (neither back reflection nor Fabry-Pérot effects) and a small thickness layer (no induced dephasing). For a macroscopic layer on the other hand, the Fabry-Pérot interference may be neglected, but the SFG process still sums up eight contributions. Among these, the direct forward process dominates in the transmission geometry because it involves the smallest phase mismatch. In all these particular situations, the equations simplify and the bulk contribution recovers the properties of one (or two) surface contribution, the conversion being quantified by the wavevector phase mismatch and the layer thickness.

In the bulk, the phase mismatch, inherent to beam propagation, cannot be laid aside. Its presence induces the most significant bulk effects experimentally measured in SFG spectra, namely the interference fringes related to the interplay between wavevector mismatch and thickness, and the phase mismatch pseudo-resonance. As the amplitudes related to the transmission phase mismatch dominate, most effects are experimentally observed in transmission (apart from semi-infinite bulks for which transmitted beams cannot be observed).

Beyond the famous cases (e.g. air-metal or dielectric-liquid two-media interfaces) where the semi-infinite bulk contribution may not be neglected and intimately mixes with the surface contributions,[11,13,18] a careful study of experimental data from finite thickness interfaces shows that the bulk effects may also there interact with, or even overwhelm, the expected surface terms. As they possess well defined properties (interference conditions, period, resonance conditions), they may be more easily disentangled from the surface response than in the semi-infinite case. Even if it requires some slight adjustment of the material properties; in particular the refractive indices, we have shown that the predicted properties match indeed the observed experimental behaviors.

Appendix A: Fresnel factors at arbitrary depth

In a general way, the SFG intensity emitted in reflection (i.e. towards medium [1]) by a surface nonlinear sheet inside an N-layer system is equal to:

$$I_R(\omega_3) = \frac{8\pi^3(\omega_3)^2}{c^3 n_3^{[1]} n_1^{[1]} n_2^{[1]} (\cos\theta_3^{[1]})^2} |\chi_{eff}^{(2)}|^2 I(\omega_1) I(\omega_2) \tag{A1}$$

where intensities are defined by $I(\omega_i) = \frac{c n_i^{[1]}}{2\pi} |\boldsymbol{E}^0(\omega_i)|^2$ with $\boldsymbol{E}^0$ the far field, $n_i^{[j]}$ and $\theta_i^{[j]}$ are the refractive index and angle of incidence of beam i (frequency ω_i) in medium [j], respectively. Angles in all media stem from angles in medium [1] following Snell's law, and SFG angle is determined by the phase matching condition (conservation of the wavevectors parallel to the interface):

$$n_1^{[1]}\omega_1 \sin\theta_1^{[1]} + n_2^{[1]}\omega_2 \sin\theta_2^{[1]} = n_3^{[1]}\omega_3 \sin\theta_3^{[1]} \tag{A2}$$

Attaching a Cartesian coordinate system to the interface, with (x,y) defining the interface planes, z the normal pointing towards medium 1 and $z = 0$ the first interface, the effective surface susceptibility is defined as:

$$\chi_{eff}^{(2)} = \sum_{\alpha\beta\gamma} F_\alpha(\omega_3) e_\alpha^{[1]}(\omega_3)\, F_\beta(\omega_1) e_\beta^{[1]}(\omega_1)\, F_\gamma(\omega_2) e_\gamma^{[1]}(\omega_2)\, \chi_{\alpha\beta\gamma}^{(2)} \tag{A3}$$

where α, β, γ stand for the Cartesian coordinates and $\boldsymbol{e}^{[1]}$ is the polarization unit vector perpendicular to wavevector $\boldsymbol{k}^{[1]}$ in medium [1]. For transmitted SFG, the equations become

$$I_T(\omega_3) = \frac{8\pi^3(\omega_3)^2}{c^3 n_3^{[N]} n_1^{[1]} n_2^{[1]} (\cos\theta_3^{[N]})^2} |\chi_{eff,T}^{(2)}|^2 I(\omega_1) I(\omega_2). \tag{A4}$$

and

$$\chi_{eff,T}^{(2)} = \sum_{\alpha\beta\gamma} F_\alpha^T(\omega_3) e_\alpha^{[N]}(\omega_3)\, F_\beta(\omega_1) e_\beta^{[1]}(\omega_1)\, F_\gamma(\omega_2) e_\gamma^{[1]}(\omega_2)\, \chi_{\alpha\beta\gamma}^{(2)} \tag{A5}$$

where the last medium of the system is labelled [N]. The Fresnel factors apply at the location where the nonlinear sheet is placed, i.e. depth $z = -z_0 \leq 0$. We recall the formulas for the reflection Fresnel factors inside layer [2] of the three layer (3L) system:[24]

$$F_x^{3L}(\omega_i) = \left[1 - r_p^{12}(\omega_i)\right] \frac{e^{ik_{i,z}^{[2]} z_0} - r_p^{23}(\omega_i) e^{2i\beta_i} e^{-ik_{i,z}^{[2]} z_0}}{1 + r_p^{12}(\omega_i) r_p^{23}(\omega_i) e^{2i\beta_i}} \tag{A6}$$

$$F_y^{3L}(\omega_i) = \left[1 + r_s^{12}(\omega_i)\right] \frac{e^{ik_{i,z}^{[2]} z_0} + r_s^{23}(\omega_i) e^{2i\beta_i} e^{-ik_{i,z}^{[2]} z_0}}{1 + r_s^{12}(\omega_i) r_s^{23}(\omega_i) e^{2i\beta_i}} \tag{A7}$$

$$F_z^{3L}(\omega_i) = \left[1 + r_p^{12}(\omega_i)\right] \frac{e^{ik_{i,z}^{[2]} z_0} + r_p^{23}(\omega_i) e^{2i\beta_i} e^{-k_{i,z}^{[2]} z_0}}{1 + r_p^{12}(\omega_i) r_p^{23}(\omega_i) e^{2i\beta_i}} \left(\frac{n_i^{[1]}}{n_i^{[2]}}\right)^2 \tag{A8}$$

where $r_{s/p}^{j,j+1}$ are the reflection coefficients at interface j between media [j] and [j+1]; $k_{i,z}^{[2]} = \frac{\omega_i}{c} n_i^{[2]} \cos\theta_i^{[2]}$; $\beta_i = k_{i,z}^{[2]} D$ and D is the thickness of layer [2]. For completeness, we give the values of coefficients A_{α_i} below:

$$A_x(\omega_i, D) = \frac{1 - r_p^{12}(\omega_i)}{1 + r_p^{12}(\omega_i) r_p^{23}(\omega_i) e^{2i\beta_i}} \tag{A9}$$

$$A_y(\omega_i, D) = \frac{1 + r_s^{12}(\omega_i)}{1 + r_s^{12}(\omega_i) r_s^{23}(\omega_i) e^{2i\beta_i}} \tag{A10}$$

$$A_z(\omega_i, D) = \frac{1 + r_p^{12}(\omega_i)}{1 + r_p^{12}(\omega_i) r_p^{23}(\omega_i) e^{2i\beta_i}} \left(\frac{n_i^{[1]}}{n_i^{[2]}}\right)^2 \tag{A11}$$

with $B_x(\omega_i) = -r_p^{23}(\omega_i)$, $B_y(\omega_i) = r_s^{23}(\omega_i)$ and $B_z(\omega_i) = r_p^{23}(\omega_i)$.

Transmission factors for the SFG beam follow from the transformation of the reflection ones according to the lines explained in Ref. 24 and read:

$$F_x^{3L,T}(\omega_3) = \left[1 - r_p^{32}(\omega_3)\right] \frac{e^{-ik_{3,z}^{[2]} z_0} - r_p^{21}(\omega_3) e^{ik_{3,z}^{[2]} z_0}}{1 + r_p^{32}(\omega_3) r_p^{21}(\omega_3) e^{2i\beta_3}} \tag{A12}$$

$$F_y^{3L,T}(\omega_3) = \left[1 + r_s^{32}(\omega_3)\right] \frac{e^{-ik_{3,z}^{[2]} z_0} + r_s^{21}(\omega_3) e^{ik_{3,z}^{[2]} z_0}}{1 + r_s^{32}(\omega_3) r_s^{21}(\omega_3) e^{2i\beta_3}} \tag{A13}$$

$$F_z^{3L,T}(\omega_3) = \left[1 + r_p^{32}(\omega_3)\right] \frac{e^{-ik_{3,z}^{[2]} z_0} + r_p^{21}(\omega_3) e^{ik_{3,z}^{[2]} z_0}}{1 + r_p^{32}(\omega_3) r_p^{21}(\omega_3) e^{2i\beta_3}} \left(\frac{n_3^{[3]}}{n_3^{[2]}}\right)^2 \tag{A14}$$

Accordingly, we have

$$A_x^T(\omega_3, D) = \frac{1 - r_p^{32}(\omega_3)}{1 + r_p^{32}(\omega_3) r_p^{21}(\omega_i) e^{2i\beta_3}} \tag{A15}$$

$$A_y^T(\omega_3, D) = \frac{1 + r_s^{32}(\omega_3)}{1 + r_s^{32}(\omega_3) r_s^{21}(\omega_3) e^{2i\beta_3}} \tag{A16}$$

$$A_z^T(\omega_3, D) = \frac{1 + r_p^{32}(\omega_3)}{1 + r_p^{32}(\omega_3) r_p^{21}(\omega_3) e^{2i\beta_3}} \left(\frac{n_3^{[3]}}{n_3^{[2]}}\right)^2 \tag{A17}$$

with $B_x^T(\omega_3) = -r_p^{21}(\omega_3)$, $B_y^T(\omega_3) = r_s^{21}(\omega_3)$ and $B_z^T(\omega_3) = r_p^{21}(\omega_3)$.

The formulas for the N-layer system may be found in Ref. 25. The factors applying inside layer [k] (defined by $z^{[k]} \leq z \leq z^{[k-1]} < 0$, thickness $d^{[k]}$, refractive index $n^{[k]}$) at $z = -z_0$

are:

$$F_x^{[k]}(z_0) = \frac{\left[e^{i\beta^{[k]}(z_0)} - r_p^{k,k+1}\xi^{[k]}e^{-i\beta^{[k]}(z_0)}\right]^\dagger \prod_{j=k+1}^{N-1}\left[1+\xi^{[j]}r_p^{j-1,j}r_p^{j,j+1}\right]^\dagger}{\prod_{j=2}^{N-1}\left[1+\xi^{[j]}r_p^{j-1,j}r_p^{j,j+1}\right]^\dagger}\prod_{j=2}^{k}\left[1-r_p^{j-1,j}\right]\prod_{j=2}^{k-1}e^{i\beta^{[j]}} \tag{A18}$$

$$F_y^{[k]}(z_0) = \frac{\left[e^{i\beta^{[k]}(z_0)} + r_s^{k,k+1}\xi^{[k]}e^{-i\beta^{[k]}(z_0)}\right]^\dagger \prod_{j=k+1}^{N-1}\left[1+\xi^{[j]}r_s^{j-1,j}r_s^{j,j+1}\right]^\dagger}{\prod_{j=2}^{N-1}\left[1+\xi^{[j]}r_s^{j-1,j}r_s^{j,j+1}\right]^\dagger}\prod_{j=2}^{k}\left[1+r_s^{j-1,j}\right]\prod_{j=2}^{k-1}e^{i\beta^{[j]}} \tag{A19}$$

$$F_z^{[k]}(z_0) = \left(\frac{n^{[1]}}{n^{[k]}}\right)^2 \frac{\left[e^{i\beta^{[k]}(z_0)} + r_p^{k,k+1}\xi^{[k]}e^{-i\beta^{[k]}(z_0)}\right]^\dagger \prod_{j=k+1}^{N-1}\left[1+\xi^{[j]}r_p^{j-1,j}r_p^{j,j+1}\right]^\dagger}{\prod_{j=2}^{N-1}\left[1+\xi^{[j]}r_p^{j-1,j}r_p^{j,j+1}\right]^\dagger}\prod_{j=2}^{k}\left[1+r_p^{j-1,j}\right]\prod_{j=2}^{k-1}e^{i\beta^{[j]}} \tag{A20}$$

where $\beta^{[k]}(z_0) = \frac{\omega}{c}n^{[k]}(z^{[k-1]}+z_0)\cos\theta^{[k]}$, and $\xi^{[k]} = e^{2i\beta^{[k]}}$ with $\beta^{[k]} = \frac{\omega}{c}n^{[k]}d^{[k]}\cos\theta^{[k]}$. The dagger (†) superscript indicates use of the ruled product: under this rule, all factors of the form $(r_{s/p}^{j,j+1})^2$ are set to 1. This gives for coefficients $A_{\alpha_i}(\omega_i, d^{[k]})$:

$$A_x(\omega_3, d^{[k]}) = \frac{\prod_{j=k+1}^{N-1}\left[1+\xi^{[j]}r_p^{j-1,j}r_p^{j,j+1}\right]^\dagger}{\prod_{j=2}^{N-1}\left[1+\xi^{[j]}r_p^{j-1,j}r_p^{j,j+1}\right]^\dagger}\prod_{j=2}^{k}\left[1-r_p^{j-1,j}\right]\prod_{j=2}^{k-1}e^{i\beta^{[j]}} \tag{A21}$$

$$A_y(\omega_3, d^{[k]}) = \frac{\prod_{j=k+1}^{N-1}\left[1+\xi^{[j]}r_s^{j-1,j}r_s^{j,j+1}\right]^\dagger}{\prod_{j=2}^{N-1}\left[1+\xi^{[j]}r_s^{j-1,j}r_s^{j,j+1}\right]^\dagger}\prod_{j=2}^{k}\left[1+r_s^{j-1,j}\right]\prod_{j=2}^{k-1}e^{i\beta^{[j]}} \tag{A22}$$

$$A_z(\omega_3, d^{[k]}) = \left(\frac{n^{[1]}}{n^{[k]}}\right)^2 \frac{\prod_{j=k+1}^{N-1}\left[1+\xi^{[j]}r_p^{j-1,j}r_p^{j,j+1}\right]^\dagger}{\prod_{j=2}^{N-1}\left[1+\xi^{[j]}r_p^{j-1,j}r_p^{j,j+1}\right]^\dagger}\prod_{j=2}^{k}\left[1+r_p^{j-1,j}\right]\prod_{j=2}^{k-1}e^{i\beta^{[j]}} \tag{A23}$$

Fresnel coefficients for the SFG beam in the transmission geometry follow by swapping the indices for reflection coefficients, i.e. $\{1, 2, \cdots, k-1, k, \cdots, N-1, N\}$ into $\{N, N-$

$1, \cdots, k, k-1, \cdots, 2, 1\}$, calculating the propagation phases from the last interface and subtracting $\sum_{j=2}^{N-1} \beta_3^{[j]}$ to account for the origin of the phases set at $z = 0$:

$$F_x^{[k],T}(z_0) = \frac{\left[e^{-i\beta^{[k]}(z_0)} - r_p^{k,k-1}\ e^{i\beta^{[k]}(z_0)}\right]^\dagger \prod_{j=2}^{k-1} \left[1 + \xi^{[j]} r_p^{j+1,j} r_p^{j,j-1}\right]^\dagger}{\prod_{j=2}^{N-1} \left[1 + \xi^{[j]} r_p^{j+1,j} r_p^{j,j-1}\right]^\dagger} \prod_{j=k}^{N-1} \left[1 - r_p^{j+1,j}\right] \prod_{j=k+1}^{N-1} e^{-i\beta^{[j]}} \tag{A24}$$

$$F_y^{[k],T}(z_0) = \frac{\left[e^{-i\beta^{[k]}(z_0)} + r_s^{k,k-1}\ e^{i\beta^{[k]}(z_0)}\right]^\dagger \prod_{j=2}^{k-1} \left[1 + \xi^{[j]} r_s^{j+1,j} r_s^{j,j-1}\right]^\dagger}{\prod_{j=2}^{N-1} \left[1 + \xi^{[j]} r_s^{j+1,j} r_s^{j,j-1}\right]^\dagger} \prod_{j=k}^{N-1} \left[1 + r_s^{j+1,j}\right] \prod_{j=k+1}^{N-1} e^{-i\beta^{[j]}} \tag{A25}$$

$$F_z^{[k],T}(z_0) = \left(\frac{n^{[N]}}{n^{[k]}}\right)^2 \frac{\left[e^{-i\beta^{[k]}(z_0)} + r_p^{k,k-1}\ e^{i\beta^{[k]}(z_0)}\right]^\dagger \prod_{j=2}^{k-1} \left[1 + \xi^{[j]} r_p^{j+1,j} r_p^{j,j-1}\right]^\dagger}{\prod_{j=2}^{N-1} \left[1 + \xi^{[j]} r_p^{j+1,j} r_p^{j,j-1}\right]^\dagger} \prod_{j=k}^{N-1} \left[1 + r_p^{j+1,j}\right] \prod_{j=k+1}^{N-1} e^{-i\beta^{[j]}} \tag{A26}$$

This leads to

$$A_x^T(\omega_3, d^{[k]}) = \frac{\prod_{j=2}^{k-1} \left[1 + \xi^{[j]} r_p^{j+1,j} r_p^{j,j-1}\right]^\dagger}{\prod_{j=2}^{N-1} \left[1 + \xi^{[j]} r_p^{j+1,j} r_p^{j,j-1}\right]^\dagger} \prod_{j=k}^{N-1} \left[1 - r_p^{j+1,j}\right] \prod_{j=k+1}^{N-1} e^{-i\beta^{[j]}} \tag{A27}$$

$$A_y^T(\omega_3, d^{[k]}) = \frac{\prod_{j=2}^{k-1} \left[1 + \xi^{[j]} r_s^{j+1,j} r_s^{j,j-1}\right]^\dagger}{\prod_{j=2}^{N-1} \left[1 + \xi^{[j]} r_s^{j+1,j} r_s^{j,j-1}\right]^\dagger} \prod_{j=k}^{N-1} \left[1 + r_s^{j+1,j}\right] \prod_{j=k+1}^{N-1} e^{-i\beta^{[j]}} \tag{A28}$$

$$A_z^T(\omega_3, d^{[k]}) = \left(\frac{n^{[N]}}{n^{[k]}}\right)^2 \frac{\prod_{j=2}^{k-1} \left[1 + \xi^{[j]} r_p^{j+1,j} r_p^{j,j-1}\right]^\dagger}{\prod_{j=2}^{N-1} \left[1 + \xi^{[j]} r_p^{j+1,j} r_p^{j,j-1}\right]^\dagger} \prod_{j=k}^{N-1} \left[1 + r_p^{j+1,j}\right] \prod_{j=k+1}^{N-1} e^{-i\beta^{[j]}} \tag{A29}$$

DATA AVAILABILITY

The data that support the findings of this study are available from the corresponding author upon reasonable request.

REFERENCES

[1]N. Bloembergen and P. S. Pershan, Phys. Rev. **128**, 606 (1962).

[2]N. Bloembergen, R. K. Chang, and C. H. Lee, Phys. Rev. Lett. **16**, 986 (1966).

[3]P. Guyot-Sionnest and Y. R. Shen, Phys. Rev. B **38**, 7985 (1988).

[4]V. Mizrahi and J. E. Sipe, J. Opt. Soc. Am. B-Optical Phys. **5**, 660 (1988).

[5]F. X. Wang, F. J. Rodríguez, W. M. Albers, R. Ahorinta, J. E. Sipe, and M. Kauranen, Phys. Rev. B **80**, 233402 (2009).

[6]A. V. Petukhov, Phys. Rev. B **52**, 16901 (1995).

[7]J. A. Maytorena, B. S. Mendoza, and W. L. Mochán, Phys. Rev. B **57**, 2569 (1998).

[8]B. S. Mendoza, W. L. Mochán, and J. A. Maytorena, Phys. Rev. B **60**, 14334 (1999).

[9]B. Busson and L. Dalstein, J. Chem. Phys. **149**, 034701 (2018).

[10]T. F. Heinz, in *Nonlinear Surf. Electromagn. Phenom.*, edited by H. E. Ponath and G. I. Stegeman (Elsevier, Amsterdam, 1991) Chap. 5, pp. 353–416.

[11]H. Held, A. I. Lvovsky, X. Wei, and Y. R. Shen, Phys. Rev. B **66**, 205110 (2002).

[12]V. Ostroverkhov, G. A. Waychunas, and Y. R. Shen, Phys. Rev. Lett. **94**, 046102 (2005).

[13]Y. R. Shen, J. Phys. Chem. C **116**, 15505 (2012).

[14]M. Okuno and T.-A. Ishibashi, J. Phys. Chem. Lett. **5**, 2874 (2014).

[15]M. Thämer, T. Garling, R. K. Campen, and M. Wolf, J. Chem. Phys. **151**, 064707 (2019).

[16]G. Gonella, C. Lütgebaucks, A. G. F. de Beer, and S. Roke, J. Phys. Chem. C **120**, 9165 (2016).

[17]P. E. Ohno, H.-F. Wang, and F. M. Geiger, Nat. Commun. **8**, 1032 (2017).

[18]W.-C. Yang, B. Busson, and D. K. Hore, J. Chem. Phys. **152**, 084708 (2020).

[19]B. Busson and A. Tadjeddine, J. Phys. Chem. C **112**, 11813 (2008).

[20]M. Okuno and T.-A. Ishibashi, J. Chem. Phys. **149**, 244703 (2018).

[21]Y.-C. Wen, S. Zha, X. Liu, S. Yang, P. Guo, G. Shi, H. Fang, Y. R. Shen, and C. Tian, Phys. Rev. Lett. **116**, 016101 (2016).

[22]N. García Rey, E. Weißenborn, F. Schulze-Zachau, G. Gochev, and B. Braunschweig, J. Phys. Chem. C **123**, 1279 (2019).

[23]X. Wei, S.-C. Hong, A. I. Lvovsky, H. Held, and Y. R. Shen, J. Physi. Chem. B **104**, 3349 (2000).

[24]B. Busson, submitted to J. Chem. Phys. (2023).

[25]B. Busson, submitted to J. Chem. Phys. (2023).

[26]M. A. Belkin, T. A. Kulakov, K. H. Ernst, L. Yan, and Y. R. Shen, Phys. Rev. Lett. **85**, 4474 (2000).

[27]R. E. Raab and O. L. de Lange, *Multipole theory in electromagnetism* (Oxford University Press, Oxford, 2005).

[28]M. Kauranen and S. Cattaneo, Prog. Opt. **51**, 69 (2008).

[29]C. Hirose, H. Ishida, K. Iwatsu, N. Watanabe, J. Kubota, A. Wada, and K. Domen, J. Chem. Phys. **108**, 5948 (1998).

[30]Y. R. Shen and V. Ostroverkhov, Chem. Rev. **106**, 1140 (2006).

[31]J. T. Murray, N. Peyghambarian, R. C. Powell, R. A. Stolzenberger, S. Jie, and B. Jassemnejad, Phys. Rev. A **49**, 4066 (1994).

[32]R. W. Boyd, *Nonlinear optics* (Academic Press, San Diego, CA, USA, 2003).

[33]M. M. Fejer, G. A. Magel, D. H. Jundt, and R. L. Byer, IEEE J. Quant. Elec. **28**, 2631 (1992).

[34]R. Haïdar, N. Forget, P. Kupecek, and E. Rosencher, J. Opt. Soc. Am. B **21**, 1522 (2004).

[35]J. Choi, J. Lee, M. Makarem, S. Huang, and S. H. Kim, J. Phys. Chem. B **126**, 6629 (2022).

[36]S. Roke and G. Gonella, Ann. Rev. Phys. Chem. **63**, 353 (2012).

[37]S. Roke, M. Bonn, and A. V. Petukhov, Phys. Rev. B **70**, 115106 (2004).

[38]A. G. F. de Beer and S. Roke, Phys. Rev. B **79**, 155420 (2009).

[39]M. J. Foster, A. P. Carpenter, and G. L. Richmond, J. Phys. Chem. B **125**, 9629 (2021).

[40]A. G. F. de Beer and S. Roke, J. Chem. Phys. **132**, 234702 (2010).

[41]A. G. F. de Beer and S. Roke, Phys. Rev. B **75**, 245438 (2007).

[42]M. Baudrier-Raybaut, R. Haïdar, P. Kupecek, P. Lemasson, and E. Rosencher, Nature **432**, 374 (2004).

[43]M. Makarem, Y. Nishiyama, X. Xin, D. M. Durachko, Y. Gu, D. J. Cosgrove, and S. H. Kim, J. Phys. Chem. B **124**, 8071 (2020).

[44]X. Zhuang, P. B. Miranda, D. Kim, and Y. R. Shen, Phys. Rev. B **59**, 12632 (1999).

[45]J. F. Gomes, K. Bergamaski, M. F. Pinto, and P. B. Miranda, J. Catalysis **302**, 67 (2013).

[46]B. Busson, M. Kauranen, C. Nuckolls, T. J. Katz, and A. Persoons, Phys. Rev. Lett. **84**, 79 (2000).

[47]P. D. Maker, R. W. Terhune, M. Nisenoff, and C. M. Savage, Phys. Rev. Lett. **8**, 21 (1962).

[48]J. Jerphagnon and S. K. Kurtz, J. Appl. Phys. **41**, 1667 (1970).

[49]N. C. J. van der Valk, P. C. M. Planken, A. N. Buijserd, and H. J. Bakker, J. Opt. Soc. Am. B **22**, 1714 (2005).

[50]G. D. Boyd and C. K. N. Patel, Appl. Phys. Lett. **8**, 313 (1966).

[51]Y. R. Shen, *The Principles of Nonlinear Optics* (Wiley, New York, USA, 1984).

[52]P. Fischer, D. S. Wiersma, R. Righini, B. Champagne, and A. D. Buckingham, Phys. Rev. Lett. **85**, 4253 (2000).

[53]A. P. Fellows, M. T. L. Casford, and P. B. Davies, J. Chem. Phys. **156**, 164701 (2022).

[54]F. Peter, Z. Physik **15**, 358 (1923).

[55]H. R. Phillip and E. A. Taft, Phys. Rev. **136**, A1445 (1964).

[56]D. F. Edwards and E. Ochoa, J. Opt. Soc. Am. **71**, 607 (1981).

[57]P. Dore, A. Nucara, D. Cannavò, G. D. Marzi, P. Calvani, A. Marcelli, R. S. Sussmann, A. J. Whitehead, C. N. Dodge, A. J. Krehan, and H. J. Peters, Appl. Opt. **37**, 5731 (1998).

[58]R. P. Mildren, "Intrinsic optical properties of diamond," in *Optical Engineering of Diamond* (John Wiley & Sons, Ltd, 2013) Chap. 1, pp. 1–34.

[59]Z. Yin, Z. Akkerman, B. Yang, and F. Smith, Diamond and Related Materials **6**, 153 (1997).

[60]U. Österberg and W. Margulis, Opt. Lett. **11**, 516 (1986).

[61]F. J. Rodríguez, F. X. Wang, B. K. Canfield, S. Cattaneo, and M. Kauranen, Opt. Express **15**, 8695 (2007).

[62]F. J. Rodriguez, F. X. Wang, and M. Kauranen, Opt. Express **16**, 8704 (2008).

[63]J. Luo, H. Huynh, C. G. Pantano, and S. H. Kim, J. Non-Cryst. Solids **452**, 93 (2016).

[64]J. Luo, J. Banerjee, C. G. Pantano, and S. H. Kim, Langmuir **32**, 6035 (2016).

[65]N. Sheth, J. Luo, J. Banerjee, C. G. Pantano, and S. H. Kim, J. Non-Cryst. Solids **474**, 24 (2017).

[66]M. Rubin, Solar Energy Materials **12**, 275 (1985).

[67]I. H. Malitson, Appl. Opt. **2**, 1103 (1963).

[68]B. Bozzini, private communication (2013).

[69]B. Bozzini, B. Busson, C. Humbert, C. Mele, P. Raffa, and A. Tadjeddine, J. Electroanal. Chem. **661**, 20 (2011).

[70]W. Guo, Z. Zhu, X. Liu, Q. Ning, Q. Song, Y. Wang, Y. He, and Z. Wang, Opt. Express **31**, 8325 (2023).

[71]H. Liu, J. Yao, and A. Puri, Opt. Comm. **109**, 139 (1994).

[72]M. Reiten, R. Cheville, and N. Halas, Optics Comm. **110**, 645 (1994).

[73]I. Tomov, R. Fedosejevs, and A. Offenberger, IEEE J. Quant. Elec. **18**, 2048 (1982).

[74]R. Eckardt and J. Reintjes, IEEE J. Quant. Elec. **20**, 1178 (1984).

[75]A. Weiner, IEEE J. Quant. Elec. **19**, 1276 (1983).

[76]A. Baronavski, H. Ladouceur, and J. Shaw, IEEE J. Quant. Elec. **29**, 580 (1993).

[77]D. J. Morrow, D. D. Kohler, and J. C. Wright, Phys. Rev. A **96**, 063835 (2017).